Investigating Actinyl Oxo Cations by X-ray Absorption Spectroscopy

Christophe Den Auwer,*[a] Eric Simoni,[b] Steven Conradson,[c] and Charles Madic[d]

Keywords: Actinides / Oxo ligands / XANES / EXAFS

Early actinide elements (from U to Am) have the ability to form linear *trans*-dioxo complexes with formal valence of the actinide being equal to (V) or (VI). For instance, the ubiquity of the uranyl cation in uranium aqueous chemistry is the basis for its very important industrial and environmental concerns. As a result, the physical chemistry of the actinyl moieties has been the subject of constantly growing investigations. Among all the spectroscopic probes, X-ray absorption spectroscopy is a particularly useful element and energy-selective technique. This article reviews the investigation of molecular actinyl complexes using both XANES and EXAFS tools. The absorption edge features have long been used to characterize the frontier orbitals of the absorbing atom. In the case of actinide cations, the L_{III} edge, located in the hard X-ray region, provides a useful fingerprint of the cation polyhedron. Tentatively, simple molecular orbital considerations together with full multiple scattering simulation codes have provided significant interpretations of the edge features. Various examples involving a distortion of the actinyl coordination sphere, starting from the aqueous species are given. Complementary structural data can be obtained in the EXAFS region of the absorption spectrum. In the literature, such molecular systems have been well documented from uranyl aqueous chemistry to neptunyl or plutonyl coordination complexes with oxygen donor ligands. Furthermore, complexation mechanisms upon absorption onto mineral surfaces have been increasingly investigated over the past few years. Overall, contribution of the XAS technique to a better understanding of the actinide bonding is demonstrated from various examples of the literature and the authors' data. Importance of the simulation codes in order to better describe the absorption features is also strongly underlined.

1. Introduction

Due to their incomplete 5f and 6d electronic subshells, the actinide elements present some unusual physical and chemical properties. Moreover, the very large atomic numbers of the actinides are also responsible for very important relativistic effects, among which the scalar effect is at the origin of the so-called lanthanidic and actinidic contraction. As a consequence, the elements from the first half of the actinide series exhibit a large number of stable or metastable formal oxidation states ranking from (III) to (VII), de

[a] CEA Marcoule, DEN/DRCP/Service de Chimie des Procédés et de Séparation,
30207 Bagnols sur Cèze Cédex, France
E-mail: christophe.denauwer@cea.fr
[b] Institut de Physique Nucléaire Orsay
91405 Orsay Cedex, France
E-mail: simoni@ipno.in2p3.fr
[c] Los Alamos National Laboratory
MST-8, Los Alamos, NM 87545, USA
E-mail: conradson@lanl.gov
[d] CEA Saclay, DEN
91191 Gif sur Yvette Cedex, France
E-mail: madic@amandine.cea.fr

Dr. Christophe Den Auwer (top, left) has completed his PhD in 1996 at the chemistry department of McGill University (Canada) and the LURE synchrotron center of Paris XI University (France). He his now a staff scientist at CEA Marcoule in charge of synchrotron radiation studies and molecular radiochemistry. Since 1997, he has been involved in the synchrotron radiation studies of a joint CNRS/CEA/EDF/ANDRA research cluster about the investigation of the physical-chemical properties of actinide elements in solution. His research interests include the electronic and structural investigation of molecular actinide and transition metal species. He has particularly focused on the use of X-ray absorption techniques using synchrotron radiation in order to probe the metal−ligand bond.

Prof. Eric Simoni (top, right) is in charge of the radiochemistry graduate studies at Paris XI University/IPN. He has completed his PhD in the Institute of Nuclear Physics of Paris XI University in 1988. He has been working in the field of the electronic structure of actinides in condensed matter and specialized in optical spectroscopy. He is now involved in the mechanistic understanding of radionuclide transport in the environment related to nuclear waste disposal and environmental contamination, using several spectroscopic techniques such as photoelectron spectroscopy (XPS), time resolved laser induced fluorescence (TRLIF) and X-ray absorption spectroscopy (XAS).

Dr. Steven Conradson (bottom, left) is a project leader in the Materials Science and Technology Division at Los Alamos National Laboratory. Beginning in 1988, he has led a major program in synchrotron X-ray studies of actinides including both X-ray absorption and scatteringmethods, determining speciation in studies of both the environmental and fundamental chemistry of actinides as well as characterizing the local structure in actinide-containing solids. His current interests beyond these include the extension of local structure and lattice distortions into the origins, attributes, and implications of nanoscale heterogeneity in crystalline materials.

Prof. Charles Madic (bottom, right) presented his PhD in 1975 at the Paris VI University, France. His PhD, concerning the solvent extraction of transuranium elements from nitric acid solutions by synergistic mixture of extractants was prepared at the Fontenay-aux-Roses Nuclear Research Center of the CEA and Paris VI University. He became a Professor at the National Institute for Training Nuclear Techniques in 1988 and Director of research at the CEA in 1995. At the beginning of the 1990s, he was nominated as French delegate at the Nuclear Science Committee of the NEA (OECD). His field of interest in research concerns the chemistry of actinide elements in relation with the reprocessing of nuclear spent fuels and the treatment of nuclear wastes. Since the beginning of the 1990s, he is in charge of research programs in these fields financed by the European Commission.

MICROREVIEWS: This feature introduces the readers to the author's research through a concise overview of the selected topic. Reference to important work from others in the field is included.

pending on the atomic number. The question of delocalized vs. localized behavior of the 5f electrons still remains a critical issue to be addressed from both experimental and theoretical points of view. For that purpose, comparisons between the properties of actinides and lanthanides or even transition metals is often a common way to study these elements, although the radial extension of the 5f wavefunctions is larger than those of the 4f wavefunctions. Consequently, the actinides behave either as itinerant d transition-like systems or as localized lanthanide-like systems.[1] Indeed, americium ($5f^7 7s^2$) is considered the first actinide in the series to exhibit rare-earth-like behavior. From the structural point of view and due to their sizeable ionic radii, the actinides exhibit a wide variety of coordination numbers and therefore, both the molecular and solid-state chemistry of these elements have been extensively investigated. According to the relatively large ionic radii, these coordination numbers are rather high (6 to 12).

From both electronic and structural points of view, investigations of actinide compounds have been performed using several different techniques such as X-ray or neutron scattering, optical and vibrational spectroscopy, NMR and Mössbauer spectroscopy. Most of this work, originating from the early 1940s has dealt with condensed matter. As one of the numerous fields of investigation, the actinide electronic structure exemplifies the specificity of the 5f orbitals. In this framework, fluorescence emission lifetime, oscillator strength measurements and Zeeman effects have been widely studied and compared with corresponding lanthanide data such as those of Nd^{3+}, Eu^{3+} and Er^{3+} in the same host material.[2−5] These studies have dealt mainly with the crystal-field parameters, the wavefunctions and the associated 5f-5f transition probabilities,[6,7] the 5f-6d energy gap[8−17] (experimental values compared to ab initio DV-Xα calculations) and the energy transfers between lanthanide and actinide ions.[18] The delocalization of the 5f electrons has mainly been investigated by Mössbauer spectroscopy (mainly on the Np element), which is an efficient tool for measuring hyperfine interactions and thus to study the electronic configuration of actinides bound in solids.[19−30] many of the actinide intermetallic compounds (monopnictides and monochalcogenides) present 5f-electron behavior analogous to the 4f electrons (NpSb, NpAs, ...) but could show itinerant behavior as for the 3d electrons ($NpCo_2Si_2$, Usb, UP, ...).[31−39]

Since the mid 1970s, X-ray absorption spectroscopy (XAS) has become widely recognized as an element-specific and non-destructive structure and electronic probe. It is of particular interest when the system under investigation is lacking crystallographic order (as in glasses, solutions or gases) and precludes the use of X-ray or neutron diffraction as the preferred structural probe. NMR and Mössbauer spectroscopy are also restricted to the use of adequate nuclei. Although the applications of XAS to material or biological sciences, for instance, have been extensive since the 1980s, its use for actinide systems is relatively recent. This is mainly due to three reasons as pointed out by Karim and co-workers in 1980:[40] the need for high-energy X-ray beams as a result of the high atomic numbers of the actinides, the lack of either reliable computed electronic parameters or model compounds and the safety requirements associated with high radioactivity of most of these elements. Despite these difficulties, XAS has now been largely applied to the structural and electronic understanding of actinide materials, as summarized by P. G. Allen or S. D. Conradson in their 1997[41] and 1998[42] reviews. See also refs.[43,44] and references herein for a larger discussion on the use of XAS in coordination or environmental chemistry.

In this article, we report on the use of the XAS technique to investigate the coordination chemistry of actinyl cations. Indeed, this technique has revealed itself as one of the unique tools for addressing the characterization of the heavy cation coordination sphere in solution or in amorphous materials. We do not intend to fully describe the theory and practice of XAS as well as the physical-chemical properties of the actinyl adducts as many books and review articles have dealt with the subject extensively.[45−49] Only a brief overview is given.

XAS is a spectroscopic technique based on the informative modulations of the X-ray absorption cross section. The electronic transitions driving the absorption cross section obey the Fermi−Golden rule in its dipolar approximation, where $i>$ is the initial state wave function of eigenvalue E_i, $|f>$ is the final state wave function of eigenvalue E_f, $\varepsilon \cdot r$ is the interaction hamiltonian in the dipolar approximation and $h\omega$ is the energy of the incoming photon [Equation (1)].

$$\mu \propto \sum_f \left|\langle i|\varepsilon . r|f\rangle\right|^2 \delta\left(E_i + \hbar\omega - E_f\right) \quad (1)$$

Because of the δ function, no quantum transition can occur before the incident photon energy $h\omega$ is at least equal to the energy of the LUMO or partially vacant authorized orbital. The dipolar transition operator results in the following transition rules for the absorption process: $\Delta L = \pm 1$; $\Delta J = 0, \pm 1$ (where L is the angular momentum term and J is the LS coupling term).

It is then convenient to divide the absorption process into two parts, depending on the incident photon energy. Above the threshold (X-ray absorption near edge structure, XANES), the photoelectron is trapped inside the absorber potential barrier and it is promoted to vacant or partially vacant bound states. As the kinetic energy of the photoelectron increases, transitions outside the potential barrier can occur towards the continuum states of the system. From ca. 100 eV above the absorption edge to ca. 1000 eV (extended X-ray absorption fine structure, EXAFS), modulations of the absorption coefficient are driven by the interference between the outgoing wave function associated with the photoelectron and the backscattered ones. The EXAFS signal χ is given as the ratio between the absorption cross section μ and the atomic absorption function μ_0 [Equation (2)].

$$\mu = \mu_0(1 + \chi) \quad (2)$$

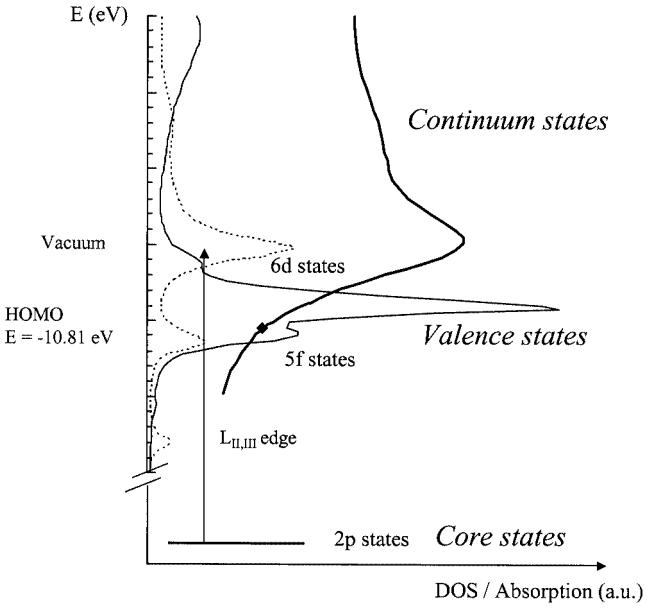

Figure 1. Schematic transitions involved in the L_{III} edge of uranyl moiety; both density of states (DOS) and absorption edge have been calculated with Feff8.1 code[50]

Figure 1 shows a schematic representation of the absorption process in the case of the L_{III} edge of UO_2^{2+}. In the primary channel picture, the $L_{II,III}$ edge corresponds to a $2p^6_{1/2,3/2}$-$nd^m \rightarrow 2p^5_{1/2,3/2}$-$nd^{m+1}$ transition (for the actinides, the first partially available d orbital is the 6d one). The threshold energy, the d and f Density of States (DOS) and the absorption spectrum have been calculated using Feff8.1 code.[50] Above the threshold, transitions occur towards the first allowed empty orbitals (6d) of uranium. Above the ionization potential (vacuum level), transitions occur towards the continuum states of the molecule.

Because most of the actinide complexes (from uranium to americium) with oxidation states higher than (IV) contain the actinyl AnO_2^{n+} ($n = 1, 2$) moieties, they are of technological and environmental importance.[41,43,51–53] Furthermore, the ubiquity of the uranyl cation in the geosphere, due to its remarkable stability, makes it one of the most extensively investigated cations within the actinide family.

The major characteristic of actinyl cations is the occurrence of quasi-linear O–An–O units with a short An–O multiple bond and a bond length ranging from 1.7 to 1.9 Å depending on the cation. This characteristic is also specific to the actinide family as only one analogue (the osmyl cation OsO_2^{2+}) is known in the d block.[54] This is good evidence of the bonding particularity that involves significant participation of the 5f orbitals in the HOMO of the AnO_2^{n+} unit. As a matter of fact, the bent structure of molecular ThO_2 versus the linear one has been the subject of numerous theoretical works questioning the extent of the 5f and 6d participation in the bonding molecular orbitals involving the two oxygen atoms.[55–59] This discussion is, however, beyond the scope of this paper as the authors would like to emphasize the role of XAS in understanding the physicochemical properties of actinyl cations.

2. Working with Actinide Elements

Although one of the major advantages of XAS is the ability to tune the absorption edge for a given element, most of the actinyl studies have dealt with L_{III} and more rarely L_I edges. Reasons for this limitation are mainly technical, as explained in the following.

The high specific radioactivity of most of the actinide elements impinges strong experimental limitations in order to comply with the safety regulations. Although dedicated research nuclear laboratories possess the experimental specific setup, this is often not the case of traditional beam line hutches at the synchrotron. Therefore, either the sample holder itself must be adequately shielded or the beam line hutch must be specifically designed. Lately, the design of dedicated beam lines at the synchrotron with appropriate shielding and/or radiation equipment has been a major improvement in the acquisition of data on actinide elements.[60–63] However, when available, the use of a specific low active radioisotope such as the uranium-238 natural isotope (^{238}U has a specific activity of $3.4 \cdot 10^{-7}$ $Ci \cdot g^{-1}$ that does not require any specific shielding) is always the preferred method. Because the X-ray beam must be transmitted through the shielding barriers, the most conveniently accessible absorption edges of the actinide series are the L edges located in the hard X-ray region from ca. 17000 to 25000 eV from U to Cf. This energy range allows successive shielding of the sample with negligible absorption of the photon beam (typically, layers of polymer or beryllium windows are used to confine the sample). Among the L edges, the L_{III} edge is very sensitive to the polyhedron structure because of the presence of strong multiple scattering contributions, as will be developed in the course of the next sections. The edge resolution is, however, limited by the short core hole life-time (giving a width of typically 7 eV at the L_{III} edge of uranium[64]). Lower energy studies at the M, N or O edges present a better edge resolution because of the larger core hole life-time and allows the 5f orbitals to be probed through the allowed dipolar transition. However, to date, these studies are scarce, given the technical difficulties in shielding the sample in the soft X-ray region. General considerations related to the manipulation of radionuclides at the synchrotron sources have been summarized in the Proceeding of the 2nd Euroconference and NEA Workhop on Speciation, Techniques and Facilities for Radioactive Materials at Synchrotron Light Sources.[61]

Another crucial issue of XAS analysis is obtaining reliable electronic model parameters [phase $\Phi(\theta, k, R) = 2kR + \varphi$, amplitude $f(\theta, k, R)$, electron mean free path $\lambda(k)$ and inelastic losses S_0^2]. Two ways of evaluating the electronic parameters are either to calculate it or to extract it from a model compound that is of known structure (i.e. the absorber to neighbor distance R and the number of neighbors

N are known) and chemically close to the material under study. On the one hand the use of experimental model compounds is the preferred method in order to obtain reliable electronic parameters. However, the difficulty in obtaining three-dimensional structures from single crystals of actinide elements is responsible for the scarcity of adequate model compounds. This statement should be tempered in the case of thorium and uranium adducts since many crystallographic data are available for these two elements. On the other hand, XAS simulation codes have become accessible for 5f elements and can be used to calculate the electronic parameters on the basis of assumed atomic coordinates.[50] In that case, several methods have been used: extrapolation from known uranium or thorium structures;[65] extrapolation from corresponding isostructural lanthanide compounds;[66] comparison with simple molecular clusters based on either quantum chemical or molecular dynamics considerations.[67] Over the past few years, the Feff code (versions 7 and 8) has been extensively tested for the actinide elements as will be reported on in the following sections. In the field of absorption edge simulation, major developments have included the implementation of self-consistent fully relativistic potential calculations based on Dirac−Hara atomic calculations and full multiple scattering treatment of the photoelectron.[68,69]

3. Actinide XANES and Electronic Structure

Near-edge spectroscopy has long been used as a fingerprint of the absorbing atom coordination geometry and electronic state. Because at low kinetic energy the photoelectron mean free path increases dramatically, the structural component of XANES can be viewed as an extension of the EXAFS energy region, given that high-order multiple scattering paths are dominant. Many works have aimed at simulating and better understanding the information included in the edge features. Depending on the relative proportion of delocalization in the valence states or electronic correlation within the final state, so-called multiple scattering or multiplet approaches have been developed.[70] Such quantitative approaches in the hard X-ray region have long been applied to spin state or local symmetry studies of transition or lanthanide metal series. On the other hand, a limited number of studies have been devoted to actinide elements, most of which deal with oxide, halide or intermetallic solid-state materials.[68,69,71−76] At the molecular level, only a few papers have addressed the simulation of actinide L edges with a multiple scattering approach.[77,78] In that framework, Ankudinov et al.[68,69] have published an extensive comparison between the series of Pu hydrates and simulations with the Feff code. Other studies have addressed this issue using both phenomenological and computational approaches.[77,78] There is still some controversy as to whether the edge features, depending on their energy (or position in the XANES spectrum) must be interpreted in terms of transitions to bound, semi-bound or continuum states. Within the absorber potential barrier, the electron is trapped above the energy threshold and both multiple scattering or molecular orbital pictures can be used as they should reflect the same underlying phenomena when electronic correlations are negligible.[79] Whether or not part of the edge features must be considered as transitions to bound states or to continuum states depends on the work function of the system. It is well known for instance that pre-edge features of the transition metal K edges can be treated as transitions to bound states made up of the hybridized unoccupied or partially occupied d states.[80−82] In the case of the L_{III} edges of the actinide elements, it has been suggested that the multiple scattering picture is more suitable to explain the edge features[69] since mixed bound-continuum states are believed to dominate the white line (WL) shape and intensity. In contrast, the L_{III} edges of the lanthanide ions exhibit a very sharp, intense and often featureless WL.[71] In the one-electron picture, this high WL ratio reflects the transition to the narrow 5d states compared to the more diffused 6d states. Additional broadening by the core hole life-time must also be taken into account as it increases with atomic number *Z*.[64,72,74] In Figure 2, the broad and intense WL, A, is typical for the actinyl L_{III} edge, from uranium to americium. Figure 2 compares the full multiple scattering (FMS) simulation of the uranyl L_{III} edge to the atomic absorption spectrum (absorption edge calculated as if the absorption atom was isolated) using the Feff-8.1 code (simulation parameters are described in ref.[83]). Calculations have been carried out on a pentagonal bipyramid cluster using self-consistency methods and muffin tin potentials, but without taking into account any sol-

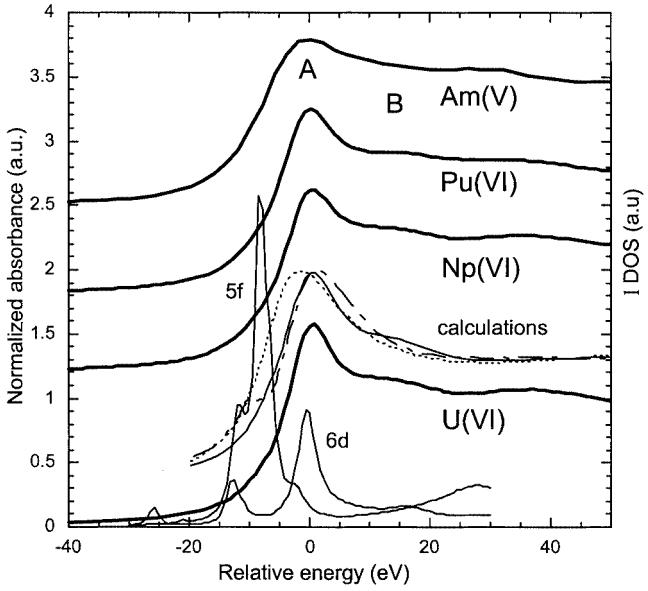

Figure 2. Experimental L_{III} edges of UO_2^{2+} (solution in perchloric acid[84]), NpO_2^{2+} (solution in perchloric acid), PuO_2^{2+} [solution of $PuO_2(NO_3)_2TBP_2$ in TBP[85]] and AmO_2^{+} [solid $K_3AmO_2(CO_3)_2$ [86]] (—); calculations (Feff-8.1) are compared to the experimental uranium edge: FMS (—), single scattering (− −) and atomic absorption (----); the $l = 2$ and $l = 3$ projected DOS is also displayed on the same relative energy scale; all the experimental spectra have been shifted in energy with respect to the calculated uranium pentagonal bipyramid edge maximum

vent effects. In addition, the *l* projected density of states (DOS) calculated with the same potentials but with no core hole, for $l = 2$ and 3, are shown on the same relative energy scale. The interpretation of A originating from a 2p to mixed 6d-continuum state transition (as the primary channel $\Delta l = +1$ of the Golden Rule) is in agreement with the 6d DOS. The similarity between the experimental WL and the atomic absorption background confirms the partial atomic character of the WL. Note that in the molecular picture, the 6d state should split under the crystal field energy (D_{5h} symmetry) but this splitting is not observed here. At about 15 eV above the WL maximum, feature B is clearly reproduced by the FMS calculation but not by the atomic absorption spectrum. A similar calculation using a single scattering approach does not account for B either. The identification of the multiple scattering (MS) paths in the FMS calculation shows that B originates from the multiple scattering paths along the *trans*-dioxo cation for both AnO_2^+ and AnO_2^{2+} moieties. This attribution of B in terms of MS contributions was previously demonstrated by Templeton[87] and Petiau[72] using polarized XAS.

Relative position of the edge is also informative as an increase in the central atom partial charge leads to a stabilization of the electronic core levels (because of the decrease in the screening effect) and a destabilization of the valence levels. If the WL is mainly of atomic-like character (as the L_{III} edge of the lanthanide for instance), the net result, everything else being equal, is a shift of the absorption edge towards higher energies as the central atom partial charge increases. Although the partial charge is often correlated to the formal oxidation state, this simplification can be misleading when different ligands yield different charge transfers between the ligands and the metal cation for a given oxidation state. This interpretation can be partially used for instance to explain the breakdown of the linear increase in edge energy (taken at the inflexion point) from An^{IV} to An^{V} [88] as a diminution in the difference of the An charge associated with the presence of covalent bonding within the *trans*-dioxo unit. More often, the absorption edge is not of pure atomic character and this leads to a mixing of both electronic and geometrical effects. This is a common ambiguity in XANES analysis as a change in the central atom oxidation state is often correlated to a change in coordination sphere. The following two examples illustrate this difficulty.

Firstly, we consider the series of Ba_2ZnAnO_6 perovskite solid-state compounds (An = U, Np, Pu) in which the actinide formal oxidation state is (VI) as in the actinyl hydrate. In these compounds, the actinide cation has been shown to be mainly ionic with an octahedral environment of 6 oxygen atoms at 2.09 Å,[89] in contrast with the rod-like structure of the actinyl cation. XANES spectra exhibit both an edge energy shift and a shape modification compared to the aqua species.[83,90] Although the edge feature can be explained in terms of transitions to the t_{2g} and e_g 6d states in an O_h symmetry, multiple scattering interpretation has also been used successfully.[83,91] In Figure 3, the *l* projected DOS calculations (Feff-8.1) of the 6d orbital matches the XANES

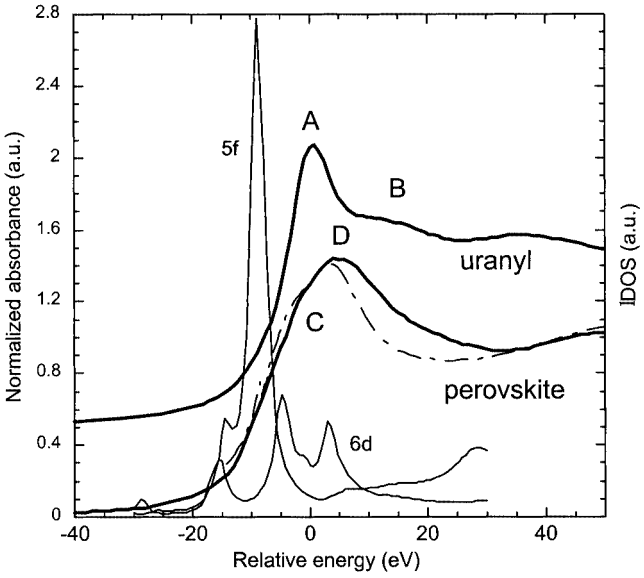

Figure 3. Experimental L_{III} edges of U^{VI} in perchloric acid and solid-state Ba_2ZnUO_6 (—) compared to FMS calculation (Feff-8.1[83]) of Ba_2ZnUO_6 (– – –); both experimental spectra have been shifted in the same relative energy scale with respect to the calculated uranium

features in terms of $t_{2g}-e_g$ splitting. The splitting energy (8 eV) is in relative agreement with previous calculations on UO_8^{13-}, AmO_8^{13-} and CmO_8^{13-} clusters (ca. 5 eV).[92] However, attribution of C and D to transitions to bound 6d states depends on the position of the ionization potential. The present calculation places the vacuum level just above C feature, meaning that D would be better described as a mixed bound−continuum state. In the MS picture, path analysis at the edge energy reveals that the low energy shoulder can be attributed to constructive interference from triangular paths within the octahedron. The high energy shift of the edge maxima from UO_2^{2+} (A) to Ba_2ZnUO_6 (D) (ca. 5 eV) would be in agreement with an increase of the uranium partial charge from uranyl to perovskite. However, attribution of D as the formal WL maximum is doubtful and the symmetry change from D_{5h} to O_h makes difficult the energy comparison with respect to the edge maximum. Also, there is a low energy shift of the inflexion point of ca. 2 eV from uranyl to perovskite, in contradiction with the above explanation. These simplistic interpretations lack a quantitative evaluation of the symmetry effect compared to the electronic effect, both effects being highly related. The energy threshold calculated by Feff-8.1 in both cases shows an increase of 1.14 eV from uranyl to perovskite and places the position of the threshold at the bottom of the absorption edge. Although this increase seems small compared to the calculation accuracy (1−2 eV [68]) it is in agreement with a significant decrease of the charge transfer (from 0.69 for uranyl to 0.35 for perovskite) calculated with the same code. At the M_v edge (3d−5f dipolar transition), the very intense WL ratio of Figure 4 reflects the more localized character of the 5f orbitals compared to the 6d ones, as well has the magnitude of the core hole attraction.[72] MS contributions

are therefore expected to be relatively weak and comparison of the WL full width at half maximum (FWHM) should reflect the trend in the 5f relative localization. Although small, the reduction of the FWHM from uranyl to perovskite (from 9.1 to 6.9 eV) agrees with the previous interpretations accounting for an increase of the uranium ionic character. Simulation of the M_V edge using a cluster based on the crystallographic structure of $UO_2(NO_3)_2{\cdot}6H_2O$ also suggests that the WL, E, is mainly driven by the final state density. Features F and G have been described in the literature [72,74] as a satellite peak (F), as an MS *trans*-dioxo contribution (G). Other authors have also observed these features in U^{VI} complexes but did not attribute it.[93] The absence of feature F in the simulation backs the interpretation of this shoulder as a multielectronic process that cannot be reproduced by the MS-based simulation code. Also, path analysis shows that G is driven by the presence of the *trans*-dioxo group and H originates from the contributions of the equatorial atoms.

As a second example, we consider the $Np^{VI}O_2^{2+}$ cation in basic and acidic solutions. In the first case, the Np atom is surrounded by 2 axial oxygen atoms at 1.82 Å and 4 equatorial oxygen atoms at 2.21 Å [94] and in the second case by 2 axial oxygen atoms at 1.75 Å and 5 equatorial oxygen atoms at 2.41 Å.[60] Both L_{III} edge spectra are compared in Figure 5 (a). From acidic to basic, they exhibit in one hand a broadening of WL A and on the other hand a shift to lower energy (-1 ± 0.5 eV for the inflexion point; -0.7 ± 0.2 eV for the WL maximum). In order to quantify the experimental changes in the edge shape and position, two series of simulations with Feff-8.1 code have been undertaken using similar parameters as those used in the case of aqueous uranyl.[84] Starting from a pentagonal bipyramid structure with the structural parameters in acidic solution, the coordination sphere has been distorted towards the structural parameters of the basic solution. Note that the symmetry is frozen at the D_{5h} point group and that neither the hydrogen atoms nor the solvent water molecules have been included in the cluster. In process I, the axial bonds have been elongated from 1.75 to 1.82 Å, the equatorial bonds being kept fixed at 2.41 Å; in process II, the equatorial bonds have been shortened from 2.41 to 2.21 Å, the axial bonds being kept fixed at 1.82 Å. The L_{III} edge simulations are compared to the experimental spectra in Figure 5 (a). The broadening of the WL from acidic to basic medium is qualitatively reproduced by the simulation. Figure 5 (b) presents the second derivative spectra calculated from the edges. Figure 5 (c) reports the first and second derivative zero points as well as the position of B shoulder. In process I, the elongation of the axial bond results in a shift of B towards A, in agreement with the relation $\Delta E{\cdot}R^2 = \text{cst}$,[72,95,96] as shown in Figure 5 (c). At the same time, both inflexion point and A are shifted to lower energy, demonstrating the sensitivity of the edge position to the coordination sphere distortion. In process II, the shortening of the equatorial distances interferes very little with the position of B, while the inflexion point and A are shifted similarly as in process I. The net result at the end of process II is an energy shift between the simulation and the experimental spectrum relative to the basic medium (Figure 5, a,b). The lower energy position of the experimental spectrum could be explained as a charge effect as the negative charge of the hydroxy ions have not been taken into account in the simulation. A higher electronic density around the neptunium atom is in agreement with a low energy shift, as observed here.

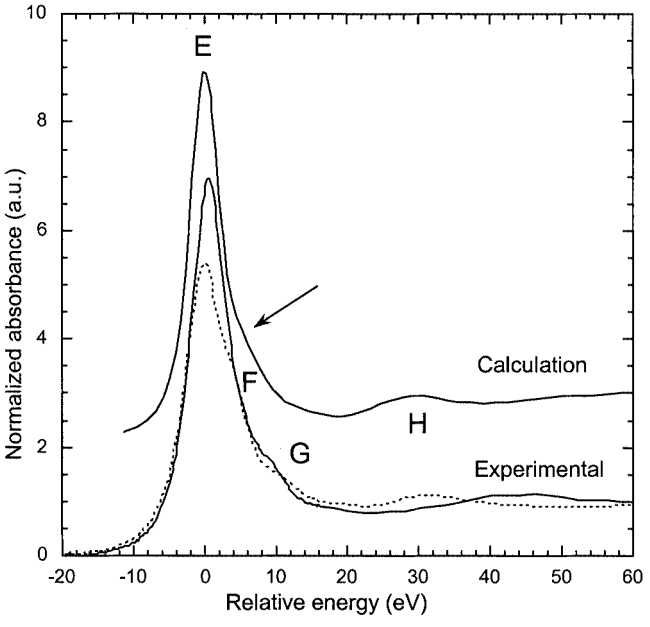

Figure 4. Experimental M_V edges of Ba_2ZnUO_6 (----) and $UO_2(NO_3)_2{\cdot}6H_2O$ (—) compared to the simulated M_V edge of $UO_2(NO_3)_2{\cdot}6H_2O$ (—);[83] all spectra have been shifted in the same relative energy scale with respect to the calculated uranium $UO_2(NO_3)_2{\cdot}6H_2O$ edge maximum

4. XAS, a Probe for Actinyl Complexes

4.1. Aqueous Actinyl Cations

The speciation of the actinyl cations in aqueous electrolytes shows a strong pH dependence and can also be affected by the presence of complexing ligands.

Although many studies have concentrated on the redox equilibrium behavior of the actinyl ions, fewer are reported on the actinide coordination sphere characterization. Lately, these data have also been complemented by quantum chemical calculations as to support the experimental results [67,97–100]. Generally speaking and in noncomplexing electrolytes, the hydrated cations can be written as $AnO_2^{n+}{\cdot}mH_2O$ (n = 1, 2) below the pH of hydrolysis and $AnO_2(OH)_{m'}^{2-m'}$ in alkaline solution. The coordination polyhedron of the actinide atom can be described as a bipyramid with the axial *trans*-dioxo atoms in the apical position and equatorial coordination geometry from trigonal to hexagonal. In acidic media, both formal oxidation states (V) and (VI) have been reported with U, Np, Pu and Am cations. As an example, the L_{III} edges of UO_2^{2+}/aq.,[84] NpO_2^{2+}/aq., PuO_2^{2+} [101] and AmO_2^{+} [86] are compared in Figure 2. All spectra are similar with a strong white line (A)

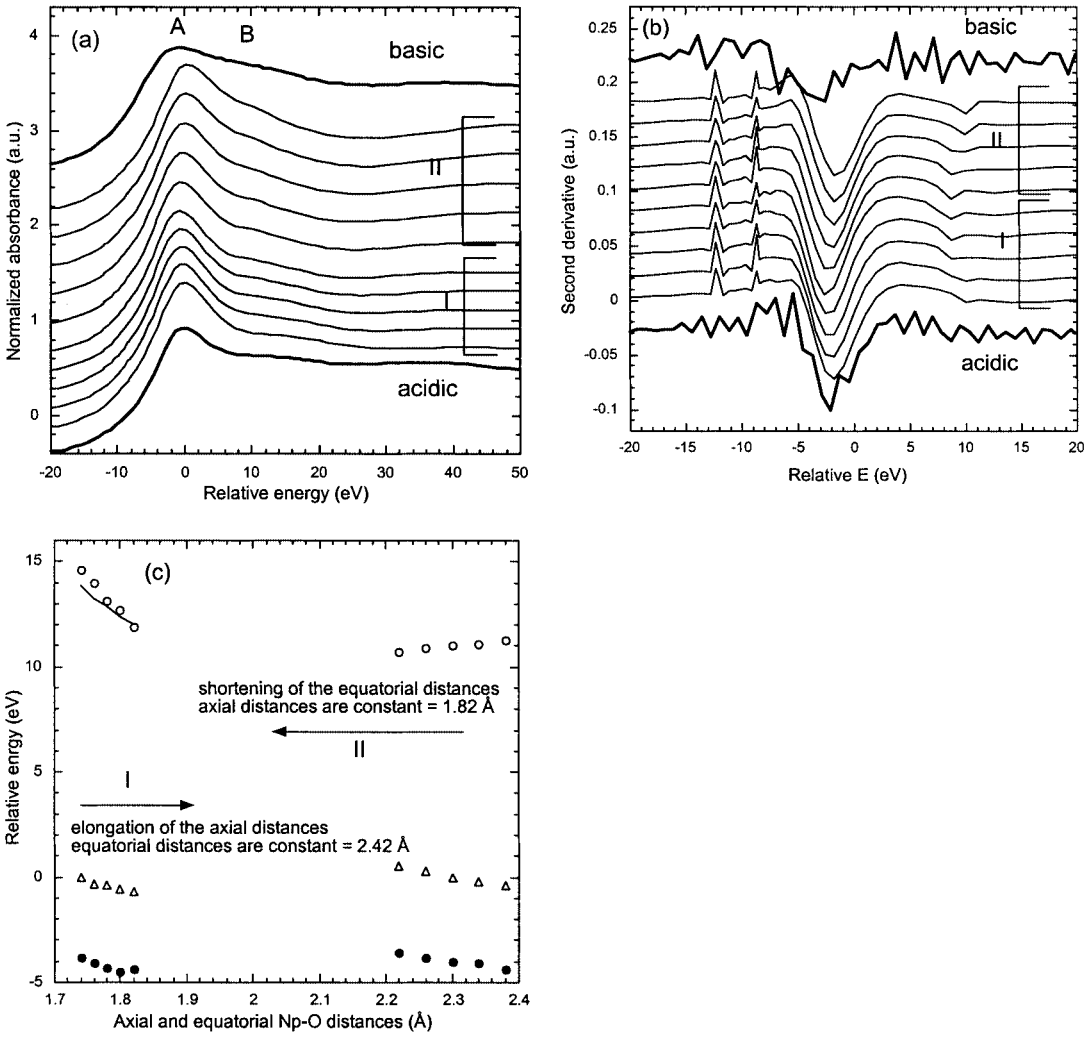

Figure 5. (a) Experimental (—) and simulated (—) L_{III} edges of $Np^{VI}O_2^{2+}$ in basic (TMA-OH) and acidic ($HClO_4$) solutions; simulations (Feff-8.1) have been carried out starting from the acidic structural parameters by successive elongation of the two apical oxygen atoms by 0.02-Å steps (process I) and by further successive shortening of the five equatorial oxygen atoms by 0.02-Å steps (process II); (b) second derivatives of the experimental (—) and simulated (—) edges; in (a) and (b) experimental and simulated spectra have been shifted in the same relative energy scale with respect to the edge maximum of the experimental acidic spectrum; (c) energy position of the simulated edge inflexion point (filled circles), maximum (triangles) and shoulder (empty circles) as a function of the axial and equatorial distances (process I and process II); the straight line (—) represents the correlation $\Delta E \cdot R^2$ = cst

and a shoulder (B) at about 15 eV above the WL maximum. Note that the relative smaller intensity of the WL in the case of the Am compound is due to the lower resolution of the beam line used to record the spectrum.

In order to address the structure of the aqueous ions, EXAFS data on aqueous actinyl ions have been well documented in the literature. Figure 6 (a,b,c) present an overview of the published data for U, Np and Pu, including the author's results. Agreement within the axial (not shown) and equatorial distances is usually satisfactory. On the contrary, it is well known that one of the major limitation of the XAS technique is the accurate determination of all the amplitude terms because they are significantly correlated. Many of the structural determinations reported in Figure 6 have used a fixed number of neighbors for the equatorial coordination shell. When floating, the parameter uncertainty is close to 20% due to amplitude transferability and experimental accuracy. This means in the case of actinyl ions that the equatorial shell is defined within plus or minus one oxygen atom.

Np and Pu are notable among the actinides for having the largest number of accessible valences, up to valence (VII). The valence (VII) state was first reported in the Russian literature[112−114] under alkaline conditions although detailed studies about the precise coordination sphere remain scarce. Due to its greatest stability for the (VII) state within the actinide family, neptunium has been the subject of most of the investigations. Recently, a few groups have provided a much more complete characterization of Np^{VII} complexes, both in the solid state and alkaline solution.[91,94,115−117] In the solid state, current XAFS[91] and single-crystal diffraction studies support the original Russian results, finding the tetraoxo configuration in the highly alkaline solutions (> 4 M OH^-) that stabilize this

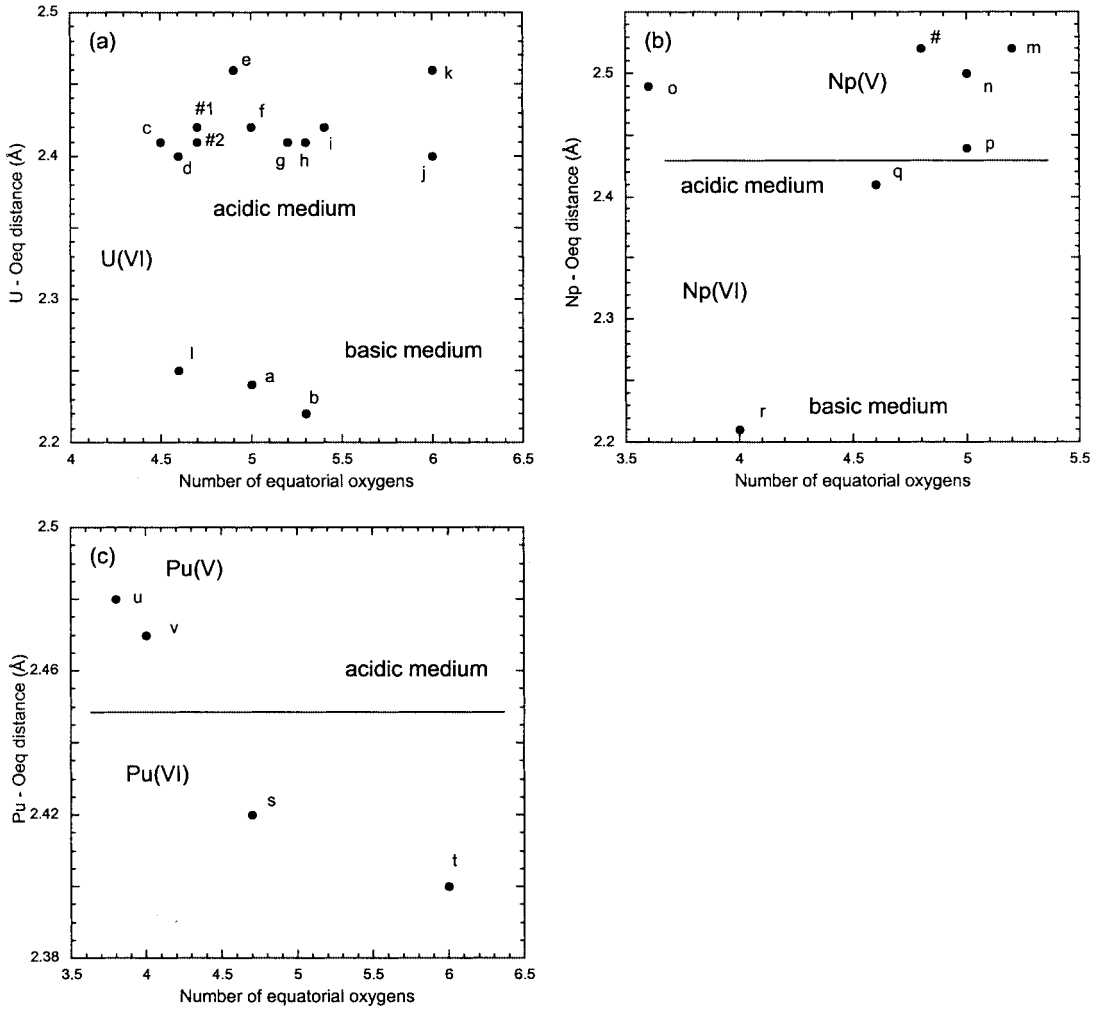

Figure 6. Actinide−oxygen equatorial distances [Å] and number of neighbors as reported from the literature: (a) uranium: a[100] − b,c[102] − d[99] − e,i[103] − f[104] − g[67] − h[105] − j[106] − k[107] − l[108] − # this work (#1 in 0.1 M $HClO_4$; #2 in 0.1 M HNO_3); (b) neptunium: the horizontal line represents the border between the Np^V/Np^{VI} domains: m[109] − n[105] − o,q[60] − p[110] − r[94] − # this work (0.01 M in $HClO_4$); (c) plutonium: the horizontal line represents the border between the Pu^V/Pu^{VI} domains; s,u[111] − t,v[42]

high oxidation state and in crystals of $Co(NH_3)_6NpO_4(OH)_2{\cdot}2H_2O$ grown from this medium. In this compound, the four Np=O oxo bonds expand to 1.85−1.90 Å, ca. 0.05 Å longer than in dioxo compounds, and the pair of *trans*-hydroxo ligands are also found at a longer 2.35−2.40 Å distance. This radical change in geometry produces a comparable change in the XANES, as shown in Figure 7. In these tetraoxo complexes the inverted ratio of short to long An−O bonds results in a shift in the relative amplitudes of the two principal features typical of the XANES of $An^{V,VI}$ with their two different An−O distances. The lower energy peak, A, corresponding to the white line in the spectra of $An^{V,VI}$ complexes decreases in intensity slightly while the higher energy feature, B, that typically occurs as a shoulder on this peak increases by a larger amount. This results in a spectrum with two resolved peaks of comparable amplitude. The separation between these features by ca. 10 eV is quite close to the energy between the peak and shoulder in the spectra of dioxo materials. This result corroborates the importance of the nearest neighbor distances as the primary origin and determinant of these two spectral features. Relative to Np^{VI} complexes, an increase in the edge energy of 1−2 eV (smaller relative to carbonato complexes, larger for hydroxo) occurs, consistent with a higher charge on the Np but also demonstrating that the incremental charge is, as expected, less than found in the oxidation from (V) to (VI). As a possible explanation, the combination of high oxidation state and OH^- donor properties promotes a higher degree of covalency and a lower charge on the central Np.

This scenario is complicated in solution, however, as observation of both dioxo and tetraoxo complexes under conditions identical to those used to prepare the tetraoxo crystals have been reported [94,115,116] by using the XAS technique. Although the Np−O distances are similar to those in Np^{VI} hydroxo complexes, the energies of the absorption edges of these samples are higher than those of Np^{VI} and close to those of the Np^{VII} tetraoxo compounds, consistent with Np^{VII} (Figure 7). However, both close inspection and curve-fits of the EXAFS indicate the presence of a small

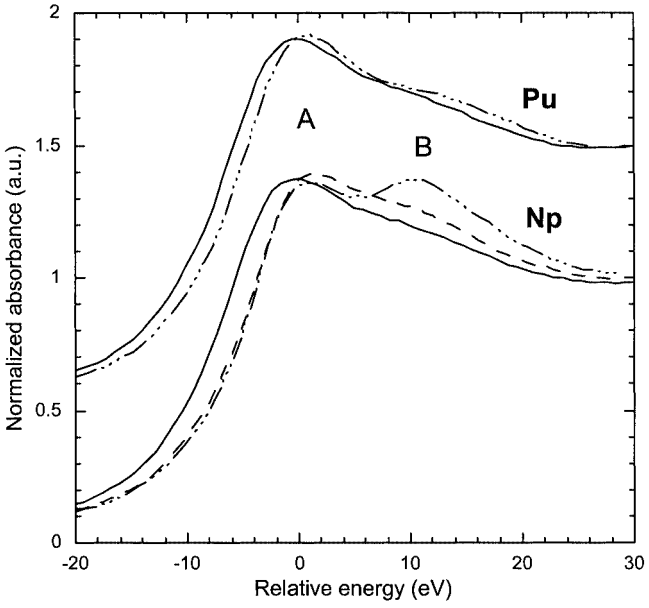

Figure 7. Experimental L_{III} edges showing both dioxo (VI) and (VII) and tetraoxo (VII) signatures of Np and Pu cations;[118] plain line spectra (—) represent the Np, Pu cations at oxidation state (VI) (in concentrated sodium hydroxide); dotted line spectra represent the Np, Pu cations at oxidation state (VII): dioxo Np^{VII} (– –) (in concentrated sodium hydroxide), tetraoxo Np^{VII} (–···–···) [in $Co(NH_3)_6NpO_4(OH)_2{\cdot}2H_2O$] and dioxo Pu^{VII} (–···–···) (in concentrated sodium hydroxide); spectra have been shifted in ordinates and energy calibrated with respect to the edge maximum of the Np^{VI} spectrum

amount of CO_3^{2-} in addition to the OH^-, so that these actually exhibit mixed hydroxy/carbonato coordination. Curve-fits show a larger number of O at the shorter Np–OH distance, which suggests an increase in number of equatorial ligands to five. The presence of strongly bound carbonate would be expected to disrupt the formation of the tetraoxo complex, resulting in the more typical dioxo geometry. This result, therefore, also demonstrates that the balance between the two geometries is delicate so that Np^{VII} is stable in both conformations, even while displaying a slight preference for the tetraoxo configuration. As would be expected from the correlation between the geometry and XANES features, the shape of the XANES of these compounds are quite similar to those of the Np^{VI} hydroxide materials, with a single peak broadened on the high energy side as the separation between the peak and shoulder decrease. The only unique signature of the Np^{VII} state is thus the somewhat higher energy of the edge. A full discussion about this issue is to be published in ref.[118] Recently, these findings have been corroborated to the Pu^{VII} system. The reversible, electrochemical production of soluble Pu^{VII} in highly alkaline media results in a dioxo complex with very slightly contracted bond lengths (0.01–0.02 Å) relative to the original Pu^{VI} starting material and a 1 eV increase in the energy of the absorption edge. At least under the conditions used in this experiment,[118] the number or order of the equatorial ligands was shown by the EXAFS to be altered in the Pu^{VII} product. No sign of CO_3^{2-} ligation is seen in the EXAFS, but only of OH^- ligation, showing that the fine balance between tetra- and dioxo configurations tips toward the latter for Pu. The Pu–O distances are also very similar between the (VI) starting material and oxidized (VII) state. Therefore, the principal effect of the higher valence on the XANES is, similarly, a 1-eV increase in the edge energy.

Studies including a variation of the electrolyte have shown that the counterion may enter the equatorial coordination sphere. Although it is usually accepted that perchlorate ions never coordinate the cation in aqueous solutions,[99] other counterions like F^-, Cl^-, CO_3^{2-} or SO_4^{2-} may form inner-sphere complexes, depending on the anion ionic strength. In the case of Cl^-/NpO_2^+ or UO_2^{2+}, it leads to a decrease of the hydration number and an increase in the Np,U–O equatorial distances as a maximum of 1.0 Cl^- (Np) or 2.6 Cl^- (U) enter the coordination sphere.[105] Similar behavior has been reported for PuO_2^{2+} with replacement of hydration water molecules with chloride ligands.[119] In the case of F^-/UO_2^{2+}, a combined EXAFS and quantum chemistry study[67] has shown that $UO_2F_n(H_2O)_{5-n}^{2-n}$ ($n = 3-5$) complexes can form within a pentagonal bipyramid geometry. Because of its ubiquity in ground water systems, carbonate ions have been extensively studied, revealing complex equilibria in solution.[120–125] Sulfate ions in binary or ternary systems have also been investigated.[126]

4.2. Coordination of Actinyl Cations with Oxygen Donor Ligands

Both steric and electronic ability of the actinide oxo cations to accept donor ligands in the equatorial plane has been at the origin of numerous coordination chemistry species.[49] As mentioned in the introduction of this article, both environmental and nuclear fuel applications of actinyl coordination chemistry have yielded a significant quantity of literature data. Most of it illustrates the use of XAS for the study of short range interactions in the solvent phase or as a complementary technique to X-ray diffraction measurements. Among the coordinating ligands of interest, oxygen donor (mono-, bi- or polydentate) ligands have been predominantly investigated. Hydroxy, carboxylate, phosphate or ether functions are often the functional groups used as donor agent in the actinyl equatorial plane.

For instance, various liquid alkyl phosphate ligands have been the subject of structural variation studies within the actinyl series from uranyl to plutonyl.[85,127] In comparison, the humic acids contain several of the above functional oxygen groups and are indeed among the most complex natural systems. Donor sites are therefore difficult to identify and alternate strategies as complexation by synthetic identified functional groups as xylose, phenylalanine or glycine are needed in order to understand the complex formation.[128] Comparison between the natural and synthetic humic acids has revealed no severe discrepancies, showing that the carboxylate groups act predominantly as monodentate ligands.[127,129] Similarly, natural wood-degradation processes lead to possible complexation by either hydroxybenzoic acids or phenols.[130] Under acidic conditions, the carboxylic

group coordinates in a bidentate mode to the uranyl cation, where under basic conditions the phenolic OH functions are the coordinating ones. Biological systems as cells have also been investigated recently. For instance, complexation of uranyl[131] and plutonyl[111] by *Bacillus sphaericus* has shown that the actinyl ion is coordinated to organophosphate groups.

Because of the relatively large atomic number of the phosphorus atom compared to C, N and H and because of the pseudo linear binding mode of the M−O=P group (M = metal), alkyl phosphates can be easily identified using EXAFS spectroscopy. Figure 8 shows the experimental and calculated EXAFS spectra and corresponding FT of solid-state compound $UO_2(NO_3)_2(TiBP)_2$ (TiBP = triisobutyl phosphate). Calculated spectra have been carried out with Feff-7 code based on the crystal structure of the compound at 77 K.[132] In this structure, the uranyl equatorial plane is filled with two bidentate nitrate ions and two monodentate phosphate ligands, the uranium atom being located on a center of symmetry. Deconvolution of the FT modulus in *n* moduli corresponding to *n* backscattering paths can be misleading if no phase is taken into account. Overall, assignment of the FT peaks in terms of backscatters is helpful, although it should be kept in mind that doing so, constructive and destructive interference are neglected. In Figure 8, the 11 paths represent the most intense backscattering process of the photoelectron. Path description is provided below with relative amplitude with respect to the one of the most intense path (a).

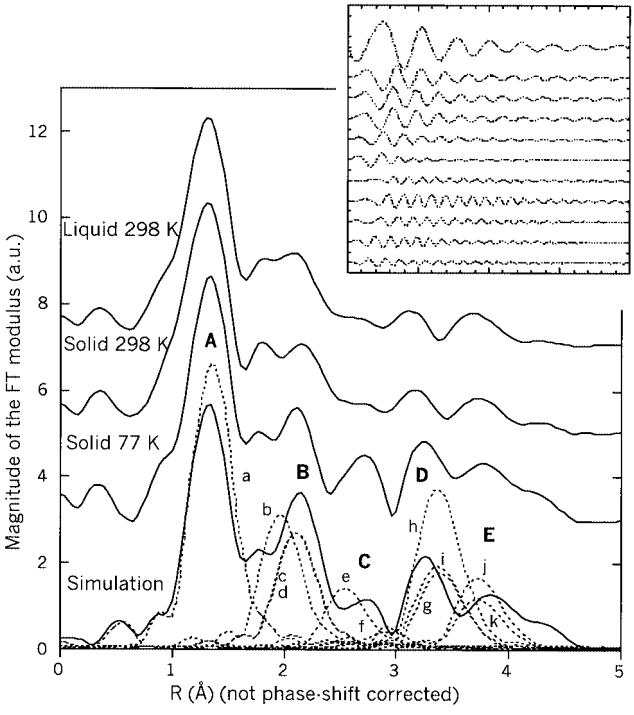

Figure 8. FT (moduli) of the EXAFS spectra of $UO_2(NO_3)_2(TBP)_2$ in TBP solution, solid-state $UO_2(NO_3)_2(TiBP)_2$ (298 K) and $UO_2(NO_3)_2(TiBP)_2$ (77 K);[85] calculated spectrum (Feff-7) of $UO_2(NO_3)_2(TiBP)_2$ is compared with moduli of each back-scattering path a to k; insert: EXAFS oscillations of each back-scattering path

Some of these paths are out of phase within each other as shown in the EXAFS spectra, leading to complex structures in the FT modulus between 2.5 and 4.5 Å (not phase-shift-corrected). For instance, peaks C and D can be mainly attributed to the two nitrogen atoms of the nitrate groups and to the phosphorus atoms of the equatorial ligands. In reality, paths e, f, g, h and i interfere. Peak E originates in a simpler way from the centrifugal oxygen atoms of the two nitrate groups. On the basis of such a path analysis, modifications of the multiple scattering amplitude factors can be used to trace deviations from linear tricenter atomic arrangements. This is the case here with the quasi linear U−O=P bonds. The quadratic dumping of the 4-leg multiple scattering path amplitude as well as the phase shift when the bond angle decreases can be used to extract bond angle information.[85]

On Figure 8, comparison is made with the FT of both solid-state $UO_2(NO_3)_2(TiBP)_2$ at 298 K and $UO_2(NO_3)_2(TBP)_2$ (TBP = tributyl phosphate) in TBP solution at 298 K. Both liquid and solid-state complexes analyzed at room temperature exhibit the same FT, in particular in the multiple-scattering 2.5−4.5-Å region. However, discrepancies with the same solid-state complex analyzed at 77 K indicate that the conformation of the uranyl coordination sphere is temperature-dependent. Decrease of the Debye−Waller factors upon temperature drop may also account for differences on the FT although data fitting has not shown any significant trend in this particular case.[85] The best fit results exhibit a nonsignificant expansion (+ 0.01 Å) of the equatorial U−O bond lengths from 77 to 298 K. At the same temperature, the solid-state and solution complexes are similar from the EXAFS point of view with 2 axial O at 1.77 Å, 2 equatorial O(phosphate) at 2.40

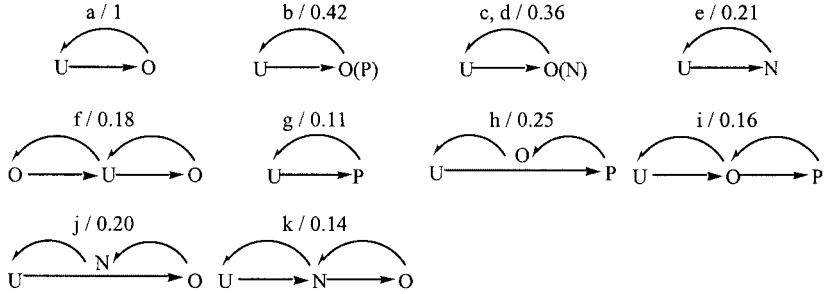

Å and 4 equatorial O(nitrate) at 2.54 Å. From U to Pu, no significant evolution of the coordination sphere can be observed. The slight coordination sphere contraction of ca. 0.03 Å upon atomic number increase can be attributed to the actinidic contraction, a direct effect of the relativistic character of the 5f electrons.[101]

Monoamide and Malonamides are also oxygen donor monodentate ligands and bind in a similar way to the uranyl equatorial plane. Few solid-state crystal structures have been published[133,134] with nitrate ligands. In Figure 9 (a,b), comparison between solid-state $UO_2(NO_3)_2(TiBP)_2$ [85] and $UO_2(NO_3)_2(DBDMBA)_2$ (*N*,*N*-dibutyl-dimethylbutaramide)[135] complexes shows minor differences. In the multiple scattering regime, peaks C, D and E are present with modulations compared to $UO_2(NO_3)_2(TiBP)_2$ because of differences in backscattering phases and amplitudes. The coordinating carboxy group plays an equivalent role as the phosphorus one, and paths g, h and i apply to peak D with a carbon atom replacing the phosphate one. Similarly with phosphate coordination, comparison between solid state and solution, both at room temperature, shows no significant difference. However, at high acidity (above ca. 5 M), protonation of the malonamide occurs and direct binding to the uranyl is inhibited.[136] Such complexes are known as ion-pairs in which outer-sphere interactions between the actinyl and the malonamide occur. Such structural modification causes dramatic changes in the EXAFS spectra as shown in Figure 9 (a,b). Symmetrization of the equatorial plane by introducing 3 bidentate nitrate ions causes a large increase in peak B of the FT. Peak D decreases in amplitude and is shifted toward smaller distances. In the absence of any U−O=C MS paths, it originates exclusively from axial oxygen atoms (path f). Overall, the U−O(nitrate) distances decrease from 2.52 Å in the inner-sphere complex to 2.48 Å in the outer-sphere complex and this contraction is explained in terms of reduced steric hindrance in the outer-sphere complex. The U−O(axial) distance is unchanged at 1.77 Å.

4.3. Actinyl Uptake from Mineral Surfaces

Actinyl interactions with mineral surfaces is of very important environmental impact, as stressed in the introduction of this article. Among the questions that XAS has addressed are inner- versus outer-sphere complexation, formation of polynuclear precipitates, and mono- vs. polydentate surface binding modes. Such data are the prerequisite to further model the interactions between the heavy metal ions and the mineral surfaces in aqueous medium. Although one of the drawbacks of the technique is to average the signal over all the possible species, tentative site-by-site data analysis has been successfully undertaken. Some of the more recent studies[84,137−140] exemplify this method, considering a topological approach between the cation coordination sphere and the surface. Such data have to be compared to the coordination processes to natural substances as humic acids, as described in the previous paragraph. The uranium cation has been the most extensively studied because of its ubiquity in the geosphere and the absence of radiological concerns[106,140−152]. However, recent work has also been devoted to thorium[138] or neptunium.[109,139] Many mineral substrates have been use, based on their occurrence in the geosphere: goethite (FeOOH), muscovite $[KAl_2(AlSi_3O_{10})(F,OH)_2]$, mackinawite (FeS),[139,144] hematite (Fe_2O_3),[137,141] ferrihydrite ($Fe_2O_3H_2O$),[150] montmorillonite $[(Na,Ca)(Al,Mg)_6(Si_4O_{10})_3(OH)_6n(H_2O)]$,[107,153] zircon ($ZrSiO_4$),[154] zirconium diphosphate (ZrP_2O_7),[142] titania (TiO_2),[84] silica,[151,155] alumina (Al_2O_3)[140] etc. In most cases, intricate binary or ternary complexes are formed between the oxo cation, the surface and the solution counterions or water molecules. Note that for all these systems the species involved in the interface chemical reactions are difficult to measure due to their low

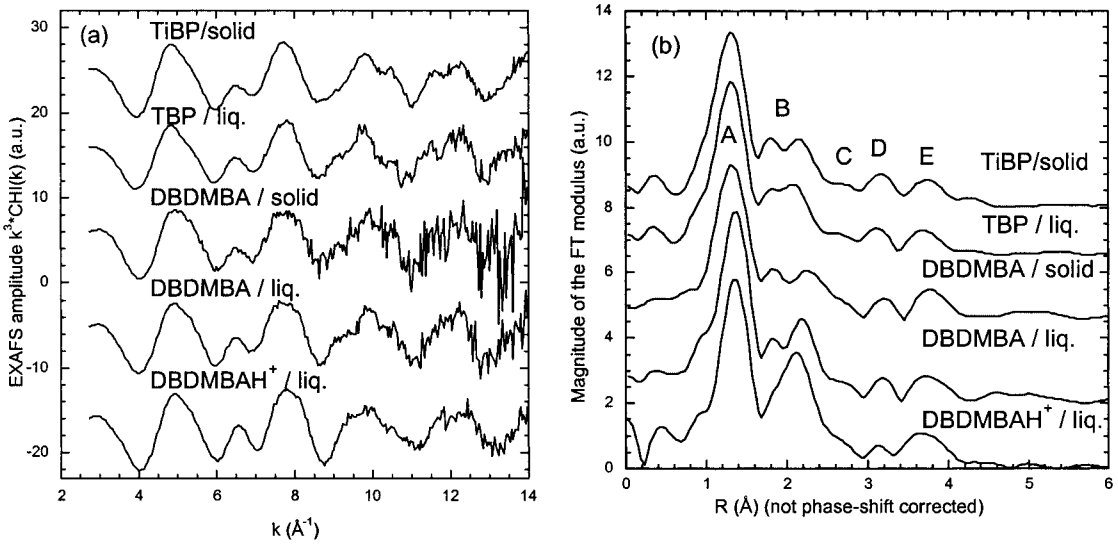

Figure 9. EXAFS spectra of solid-state compound $UO_2(NO_3)_2(TiBP)_2$, $UO_2(NO_3)_2(TBP)_2$ in TBP solution,[85] solid-state $UO_2(NO_3)_2(DBDMBA)_2$, $UO_2(NO_3)_2(DBDMBA)_2$ and $UO_2(NO_3)_3^-DBDMBAH^+$ in DBDMBA;.[135] all spectra were recorded at 298 K; (a) raw EXAFS oscillations and (b) corresponding modulus of the Fourier transform

concentration on the solid surface. Participation of the counterion to the surface complex depends on its chelating ability under the sorption conditions.

The redox chemistry of uranium in aqueous solution is predominantly governed by the +VI oxidation state (the +VI/+IV potential with respect to the standard electrode is equal to 0.27 V). As a consequence, no reduction to the +IV oxidation state is expected upon sorption under atmospheric conditions as confirmed by the invariance of the uranium L_{III} edges observed in most of the above references. Similarly, the +V oxidation state is conserved when NpO_2^+ is sorbed onto goethite (FeOOH).[109] Conversely, when mackinawite (FeS) is used as a substrate, reduction of Np^V to Np^{IV} has been observed.[139] The authors have observed a similar behavior when PuO_2^{2+} is sorbed onto thorine (ThO_2): reduction of the plutonium oxidation state from +VI to +IV occurs. This phenomenon is not explained to date. Indeed, no redox reaction can occur between the plutonium species and the tetravalent thorium as it appears with iron substrates. The physico-chemical parameters at the solid/solution interface such as pH, redox potential, structure of the water molecules, may be different than those in the bulk solution, which could change drastically the radionuclide's chemical properties at the interface. Therefore, careful investigation of the microscopic properties of this interface should be carried out. In Figure 10, examples of EXAFS spectra of UO_2^{2+}/H_2O/substrate (substrate = $LaPO_4$, ZrP_2O_7 and TiO_2)/surface complexes are presented. Table 1 summarizes the structural parameters (the first uranium coordination sphere) of surface complexes published in the literature. Confirming the XANES results, the uranyl entity is conserved in all cases. When complexing counterions are present, such as carbonate anions, ternary inner-sphere complexes can be formed with the surface and the counterion.[137,141,151] The final stoichiometry often depends on the sorption conditions (pH, concentration in the solution). In presence of perchlorate ions, no inner-sphere complex with the counterion has been published to date. On the average, the equatorial uranium coordination number ranges from 5 to 6 as in aqueous uranyl. When a two-shell fit of the equatorial oxygen atoms is performed, a shorter bond length is observed between the uranium atom and the surface than between the uranium atom and the outer oxygen atoms (carbonate oxygen atoms,[137] water oxygen atoms[84,142,151,154–156]). For example, the Fourier transform of the EXAFS spectrum, corresponding to the U^{VI}/ZrP_2O_7 system, exhibits two equatorial oxygen atoms contributions and another one arising from the phosphorus atoms. The $U-O_{surf.}$ (2.33 Å) and U–P (3.60 Å) distances and the $O_{surf.}-P-O_{surf.}$ (110°) and P–O–P (150°) angles indicate clearly that the two oxygen atoms on the surface (associated to the shorter bond length) cannot belong to only one P_2O_7 surface group, but to two different ones.[142] A similar structural investigation has been carried out with the same metal ion on the $LaPO_4$ substrate. One phosphorus atom has been found at 2.74 Å. In that case, according to the bond lengths $U-O_{surf.}$ (2.31 Å) and P–O (at 1.50 Å in the PO_4 group), the $U-O_{surf.}-P$ angle is around 90°. Consequently, if the two oxygen atoms ($U-O_{surf.}$ at 2.31 Å) belong to the same PO_4 surface group, the $O_{surf.}-P-O_{surf.}$ angle should be around 114°, which is a reasonable value for the PO_4 tetrahedron. Therefore, it is assumed that the uranyl ion is complexed with only one PO_4 surface group. Moreover, as the phosphorus atom is at only 2.74 Å from the uranium atom, this indicates that there is no water molecule layer between the sorbed uranyl ion and the surface and thus that this ion is sorbed as an inner-sphere complex.[156] Nevertheless, the data from Waite et al.[150] seem to contradict this kind of interpretation with a reverse order of the distances. EXAFS studies have been performed on totally different substrates such as montmorillonite clay as well. By comparing the EXAFS data for uranyl ions in solution and sorbed onto this clay, it has been possible to distinguish different sorption mechanisms depending on the pH value of the suspension. For instance, for a pH value equal to 5, the EXAFS spectrum of loaded uranyl is identical to the one corresponding to the uranyl ions in solution, which demonstrates that these ions are sorbed as an outer-sphere complex onto the ion-exchange interlayer site of the clay.[106]

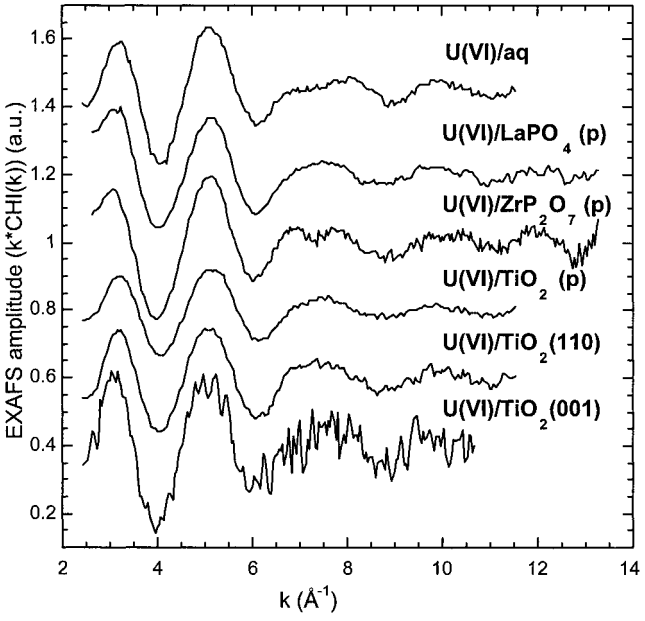

Figure 10. Raw EXAFS spectra of uranyl uptake from polycrystalline $LaPO_4$, ZrP_2O_7, TiO_2 powders[84,142,156] and single crystal of the (110) and (001) planes of TiO_2;[84] the spectrum of starting uranyl solution in perchloric acid is also displayed

As demonstrated by the growing number of sorption/XAS references, the use of polycrystalline substrates is essential to pin down the sorption mechanisms. Site-by-site interpretation of the sorption sites has even been attempted.[137,157] However, in order to better describe these surface sites, the use of crystallographic plane substrates allows a real site-by-site investigation of the surface complexes.[147,148] In the case of the uranyl oxo cation, advantage of the linear polarization of the synchrotron light has been taken in order to seek the uranyl rod orientation on the surface. Such experiment is known as Grazing Incidence

Table 1. Uranium−oxygen bond lengths [Å] in various uranyl−surface complexes as given in the literature; only binary UO_2^{2+}/H_2O/substrate complexes are summarized

Sample[a]	Axial	Equatorial (out)[b]	Equatorial (surface)	Ref.
U^{VI}/aq.	*2.0(−)*[c] O−1.77(1)	4.7(3) O −2.42(1)		[84]
U^{VI}/LaPO4	2.1(4) O−1.77(1)	1.8(4) O −2.47(2)	2.4(5) O −2.31(2)	[156]
$U^{VI}/ZrSiO_4$	2.3(4) O−1.81(2)	1.9(4) O −2.54(2)	3.1(6) O −2.36(2)	[154]
U^{VI}/ZrP_2O_7	*2.0(−)* O−1.76(2)	3.0(5) O −2.46(2)	2.1(5) O −2.33(2)	[142]
U^{VI}/rutile	*2.0(−)* O−1.79(1)	3.1(1) O −2.49(3)	2.5(4) O −2.33(2)	[84]
U^{VI}/TiO_2(110)	*2.0(−)* O −1.78(1)	2.9(2) O −2.46(1)	2.1(2) O −2.31(1)	[84]
U^{VI}/TiO_2(001)[d]	*2.0(−)* O −1.77(1)	5.5(14) O −2.43(2)		[84]
U^{VI}/goethite	2.0(10) O −1.80(2)	5.0(10) O −2.40(2)		[144]
U^{VI}/lepidocrocite	2.0(10) O −1.80(2)	4.0(10) O −2.40(2)		[144]
U^{VI}/muscovite	2.0(10) O −1.80(2)	4.0(10) O −2.35(2)		[144]
U^{VI}/mackinawite	2.0(10) O −1.81(2)	4.0(10) O −2.40(2)		[144]
U^{VI}/montmorillonite[d]	*2.0(−)* O −1.79(2)	4.6(−) O −2.44(2)		[107]
U^{VI}/ferrihydrite	*2.0(−)* O −1.80(2)	3.0(−) O −2.35(2)	2.0(−) O −2.52(2)	[131]
U^{VI}/FeOOH	*2.0(−)* O −1.79(2)	5.0(10) O −2.35(2)		[152]
U^{VI}/montmorillonite[d]	*2.0(−)* O −1.79(1)	5.4(8) O −2.43(1)		[155]
U^{VI}/silica	*2.0(−)* O −1.78(1)	3.0(9) O −2.46(3)	2.1(6) O −2.28(2)	[155]

[a] Details about sorption conditions are given in the corresponding reference. In case of varying parameters such as pH or stock solution concentration, only one result is reported in the Table. [b] Distinction between surface-bonded and outer oxygen atoms is provided when a two-shell fit is provided. [c] Numbers in *italic* correspond to fixed or linked variables. [d] Outer-sphere complex.

XAS (GXAS) and its application to actinide chemistry is relatively new.[84,143] In a general sense, GXAS is based on the variation of the apparent number of neighbors with the angle between the electric field and the chemical bond.[158] Figure 11 shows the calculated effect of polarization on the sorption orientation of UO_2^{2+} onto the (011) plane of rutile. The modulations of feature B associated with the *trans*-dioxo unit are monitored by the angle between the O=U=O bond vector and the electric field vector: maximum intensity when both vectors are collinear, minimum intensity when both vectors are normal to each other. In comparison with the calculation, the parallel and perpendicular experimental measurements exhibit a slight decrease of feature B.[84] The small difference between the two measurements suggests that the uranyl rod sorbs quasi parallel to the surface, deviation from ideality being attributed to surface defects.[159]

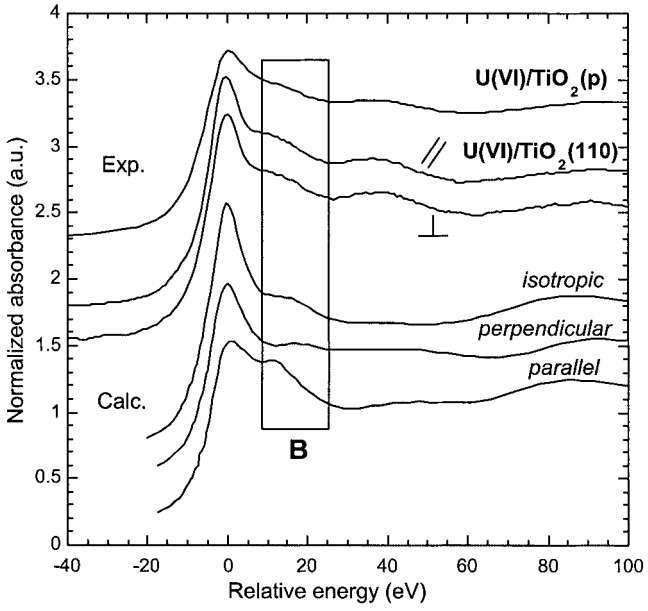

Figure 11. Uranium L_{III} edge experimental spectra of U^{VI}/TiO_2(p) and U^{VI}/TiO_2(110); U^{VI}/TiO_2(p) corresponds to an isotropic measurement; U^{VI}/TiO_2(110) has been measured with the electric field vector ε parallel (∥) and perpendicular (⊥) to the (110) surface;[84] comparison with uranium L_{III} edge simulated spectra (Feff-8.1) of $UO_2(O)_5^{2+}$ and $UO_2(O)_5$ cluster onto the TiO_2 (110) surface in the parallel and perpendicular configuration of the oxo cation bond vector with respect to ε ; for clarity, spectra have been shifted in ordinates and energy calibrated with respect to the edge maximum

EXAFS data analysis of the uranyl sorbed onto the (110) plane shows a splitting of the equatorial U−O bond lengths between U−O(surface) and U−O(out). Two possible sorption sites are available for bidentate complexation on the (110) surface: shared-edge distorted TiO_6 polyhedra and shared-summit polyhedra. Both sites are present in the surface complexes in proportions that are unknown from data analysis. Figure 12 shows a schematic representation of the surface complex in the case of the shared-edge sorption site of the (110) surface. The structural parameters are similar to the one obtained from uranyl sorption on polycrystalline

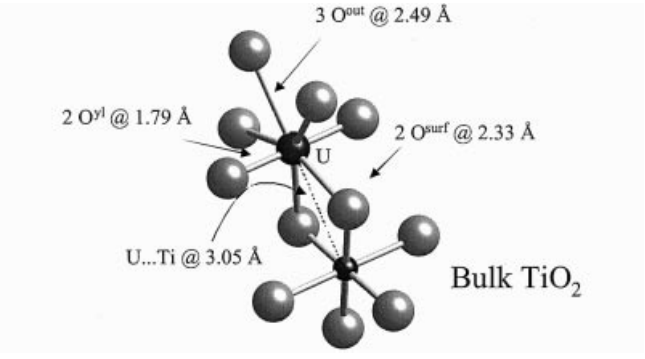

Figure 12. From EXAFS data analysis, schematic representation of the uranyl surface complex on the (110) surface of TiO_2; only the shared-edge site is represented[84]

rutile (Table 1). The shortening of the U−O equatorial bond from 2.42 Å for aqueous uranyl to 2.32 Å for U−O(surface) suggests an increase in covalency of the U−O(surface) bond. This would not be surprising, taking into account the lack of coordination for the rutile surface oxygen atoms and the possibility of charge delocalization along the surface.

5. Summary

This overview on structural and electronic aspects of actinide molecular chemistry, although limited, has hopefully demonstrated the advantages of XAS for such chemical systems. Since the actinide elements are electron-rich cations from high atomic numbers, they bear remarkable chemical properties, from the availability of many stable oxidation states to the formation of large coordination polyhedra. Such properties demonstrate the richness of the actinyl chemistry; they also underline the intricacy of working with actinide cations.

Two major issues have been schematically addressed in this article. The first one deals with acute understanding of the actinyl electronic properties. Clearly the XAS probe by itself will not fully describe the electronic valence states of the molecule and a palette of complementary techniques and calculations must be employed. Coupling simulation codes to experimental results is also essential. In that sense, the selection of various transition channels from core spectroscopy to higher primary quantum numbers is a unique tool based on the tinability of the synchrotron radiation. Photoelectron or photoemission spectroscopy are examples of electronic probes based also on the interaction of a photon with the electronic cloud. In all cases, the key approximations that must be made for simulation purposes are driven by the final state. Although the relative qualitative evolution of the features driven by the absorption processes in homogeneous series of complexes is most often understood, absolute qualitative values are much more difficult to obtain. One of the major difficulties lies in the evaluation of the structural and electronic contributions to the absorption edge, both being highly related. In that sense, increased accuracy in the calculation results, such as Fermi levels, should be particularly helpful. The development of full multiple scattering codes can be considered as one of the major milestones in the field, although progresses must be carried out in the definition of the scattering potentials.

The second issue deals with the high energy part of the absorption process, where modulations of the absorption coefficient is related to the spatial arrangement around the absorbing atom. Although the single backscattering processes describe adequately the first coordination sphere, they are of limited information beyond this shell and multiple scattering processes must be taken into account. Accurate geometrical information can also be drawn from the multiple scattering paths as their phases and amplitudes are affected by the relative bond angles and distances. Finally, coupling with quantum chemistry is essential in order to validate or favor one of the geometrical models deduced from the EXAFS data. One of the major difficulties to be pointed out occurs when several species or conformations are present. This is a common case in solution coordination chemistry when either labile complexes or low equilibrium constants are encountered. As a result, the data analysis accuracy is limited by an increasing number of fitting parameters.

From speciation to simulation, XAS has proven to be one of the useful probes for actinyl chemistry. As suggested in this article, limitation of XAS data analysis to phenomenological aspects is often restrictive and coupling with calculation codes should help to quantify the links between absorption processes and electronic properties.

Acknowledgments

This research was mainly carried out at the Laboratoire d'Utilisation du Rayonnement Electromagnétique (Orsay, France) a national user facility operated by CEA/CNRS/MR and the Stanford Synchrotron Radiation Laboratory (Stanford, USA), a national user facility operated by Stanford University on behalf of the U.S. Department of Energy, Office of Basic Energy Sciences. The authors are particularly grateful to the beam line scientists and health physicists of LURE for their constant help, support and advice. They would like also to acknowledge the beam line scientists of SSRL and health physicists supported by the Seaborg Institute at LANL. Many fruitful discussions with J. J. Rehr, A. Ankudinov and C. Cartier dit Moulin played an important part in this work and the authors would like to thank them for their help. This work has been financially supported by CEA/DEN, PRACTIS (France) and by DOE OBES Division of Chemical Sciences under Contract W-7405 (USA).

[1] A. J. Freeman, J. B. Darby, Jr., *The Actinides: Electronic structure and related properties*, Academic Press, New York, **1974**, vols. I, II.
[2] M. Karboviak, J. Drozdzynski, S. Hubert, E. Simoni, W. STREK, *J. Chem. Phys.* **1998**, 108−124, 10181−10188.
[3] P. A. Tanner, *J. Mol. Struct.* **1995**, *355*, 299−306.
[4] M. Karboviak, E. Simoni, J. Drozdzynski, S. Hubert, *Acta Phys. Pol.* **1996**, *A90*, 367−370.
[5] M. Karboviak, J. Drozdzynski, K. M. Murdoch, N. M. Edelstein, S. Hubert, *J. Chem. Phys.* **1997**, *106*, 3067−3075.
[6] E. Simoni, M. Louis, S. Hubert, M. F. Reid, *J. Phys. II* **1995**, *5*, 755−764.
[7] J. C. Krupa, E. Simoni, J. Systma, N. M. Edelstein, *J. Alloys Compd.* **1994**, *213*, 471−474.
[8] E. Simoni, M. Louis, S. Hubert, S. Xia, *Opt. Mater. (N. Y.)* **1995**, *4*, 641−650.
[9] Y. Tahri, H. Chermette, N. El Khatib, J. C. Krupa, E. Simoni, *J. Less-Common Met.* **1990**, *158*, 105−116.
[10] L. J. Nugent, R. D. Baybartz, J. L. Burnett, J. L. Ryan, *J. Inorg. Nucl. Chem.* **1971**, *33*, 2503−2530.
[11] L. J. Nugent, R. D. Baybartz, J. L. Burnett, J. L. Ryan, *J. Phys. Chem.* **1973**, *77*, 1528−1538.
[12] W. T. Carnall, H. M. Crosswhite, J. Crosswhite, J. Hessler, N. M. Edelstein, J. C. Conway, G. V. Shalimoff, R. Sarup, *J. Chem. Phys.* **1980**, *72*, 5089−5096.
[13] R. Mcdiarmid, *J. Chem. Phys.* **1976**, *65*, 168−173.
[14] D. D. Koelling, D. E. Ellis, R. J. Barlett, *J. Chem. Phys.* **1976**, *65*, 3331−3340.
[15] D. E. Ellis, A. Rosen, V. A. Gubanov, *J. Chem. Phys.* **1982**, *77*, 4051−4060.

[16] K. Pierloot, A. Renders, G. L. Goodman, D. Devoghel, C. Gorller-Walrand, L. G. Vanquickenborne, *J. Chem. Phys.* **1991**, *94*, 2928−2939.
[17] P. J. Hay, W. R. Wadt, L. R. Kahn, R. C. Raffenetti, D. H. Phillips, *J. Chem. Phys.* **1979**, *71*, 1767−1779.
[18] M. Louis, S. Hubert, E. Simoni, J. Y. Gesland, *Opt. Mater. (N.Y.)* **1996**, *6*, 121−127.
[19] J. Gal, M. Kroup, Z. Hadari, I. Nowik, *Phys. Rev. B* **1977**, *16*, 3913−3920.
[20] J. Gal, S. Fredo, Z. Hadari, J. L. Buevoz, C. de Novion, *J. Magn. Magn. Mater.* **1979**, *10*, 100−108.
[21] J. Gal, C. Musikas, J. Jové, M. Pagès, I. Nowik, *Phys. Rev. B* **1981**, *23*, 4324−4330.
[22] B. D. Dunlap, G. M. Kalvius, *J. Phys., Colloq. C4* **1979**, *40*, 192−200.
[23] B. D. Dunlap, G. H. Lander, *Phys. Rev. Lett.* **1974**, *33*, 1046−1050.
[24] H. Abazli, A. Cousson, J. Jové, M. Pagès, M. Gaspérin, *J. Less-Common Met.* **1984**, *96*, 23−31.
[25] H. Abazli, A. Cousson, J. Jové, M. Pagès, *J. Fluorine* **1980**, *16*, 647−651.
[26] T. Thévenin, J. Jové, M. Pagès, D. Damien, *Sol. State Commun.* **1981**, *40*, 1065−1072.
[27] D. G. Karraker, J. A. Stone, *Inorg. Chem.* **1979**, *70*, 2041−2050.
[28] D. G. Karraker, J. A. Stone, *Inorg. Chem.* **1980**, *19*, 3545−3552.
[29] D. G. Karraker, J. A. Stone, *Phys. Rev. B* **1980**, *22*, 111−120.
[30] D. D. Bodé, J. F. Wild, E. K. Hulet, *J. Inorg. Nucl. Chem.* **1976**, *38*, 1291−1299.
[31] D. Damien, A. Wojakowski, W. Müller, *Inorg. Nucl. Chem. Lett.* **1976**, *12*, 441−450.
[32] D. Damien, R. G. Haire, J. R. Peterson, *J. Phys. Colloq. C4* **1979**, *40*, 95−100.
[33] J. P. Charvillat, D. Damien, A. Wojakowski, *Rev. Chim. Miner.* **1977**, *14*, 178−189.
[34] A. Wojakowski, D. Damien, *J. Less-Common Met.* **1982**, *83*, 263−271.
[35] G. Calestani, J. C. Spirlet, J. Rebizant, W. Müller, *J. Less-Common Met.* **1979**, *68*, 207−212.
[36] T. Thévenin, M. Pagès, A. Wojakowski, *J. Less-Common Met.* **1982**, *84*, 133−140.
[37] A. Blaise, D. Damien, J. Mulak, *Phys. Status Solidi* **1982**, *72*, K145−K150.
[38] T. Thévenin, J. Jové, M. Pagès, *Hyperfine Interact.* **1984**, *20*, 173−179.
[39] Y. Héry, D. Damien, J. P. Charvillat, *Radiochem. Radioanal. Lett.* **1979**, *37*, 17−23.
[40] D. P. Karim, P. Georgopoulos, *Nucl. Tech.* **1980**, *51*, 162−168.
[41] P. G. Allen, J. J. Bucher, M. A. Denecke, N. M. Edelstein, N. Kaltsoyannis, H. Nitsche, T. Reich, D. K. Shuh, *Synchrotron Radiation Techniques in Industrial, Chemical and Material Sciences* (Ed.: D'Amico), Plenum Press, **1996**, p. 169−185.
[42] S. D. Conradson, *Appl. Spectrosc.* **1998**, *52*, 252−279.
[43] R. J. Silva, H. Nitsche, *Radiochim. Acta* **1995**, *70/71*, 377−396.
[44] J. E. Penner-Hahn, *Coord. Chem. Rev.* **1999**, *190/192*, 1101−1123.
[45] B. K. Teo, *Basic Principles and Data Analysis*, Springer Verlag, Berlin, **1986**.
[46] A. Bianconi, L. Incoccia, S. Stipcich, *EXAFS and Near Edge Structure, Proceedings of the International Conference, Frascati, Italy 1982*, Springer Verlag, New York, **1983**.
[47] J. Stöhr, *NEXAFS Spectroscopy*, Springer Verlag, New York, **1992**.
[48] J. J. Rehr, R. C. Albers, *Rev. Mod. Phys.* **2000**, *72*, 621−654.
[49] K. W. Bagnall, *Comprehensive Coordination Chemistry* (Ed.: G. Wilkinson), Pergamon Press, **1987**, vol. 7, chapter 40.
[50] J. J. Rehr, A. L. Ankudinov, *J. Electron Spectrosc. Relat. Phenom.* **2001**, *114−116*, 1115−1121 and references herein.
[51] C. Hennig, T. Reich, H. Funke, A. Roβberg, M. Rutsch, G. Bernhard, *J. Synchrotron Radiat.* **2001**, *8*, 695−697.
[52] W. W. Schulz, L. L. Burger, J. D. Navratil, *Science and Technology of Tributylphosphate*, CRC-Press Inc., Boca-Raton, Florida, USA, **1990**, vol. III.
[53] M. Viala, M. Salvatores, *Proceedings of the GLOBAL'95 Conference*, Versailles, France, **1995**, vol. I, p. 11−14.
[54] N. Kaltsoyannis, P. Scott, *The f elements*, Oxford Science Publisher, Zeneca, **1999**.
[55] L. Gagliardi, B. O. Roos, P-A. Malmqvist, J. M. Dyke, *J. Phys. Chem. A* **2001**, *105*, 10602−10606.
[56] P. J. Hay, R. L. Martin, G. Schreckenbach, *J. Phys. Chem. A* **2000**, *104*, 6259−6270.
[57] P. Pyykkö, L. J. Laakkonen, K. Tatsumi, *Inorg. Chem.* **1989**, *28*, 1801−1805.
[58] M. Pepper, B. Bursten, *Chem. Rev.* **1991**, *91*, 719−741.
[59] R. G. Denning, *Struct. Bonding* **1992**, *79*, 217−276.
[60] T. Reich, G. Bernhard, G. Geipel, H. Funke, C. Heining, A. Roβberg, W. Matz, N. Schell, H. Nitsche, *Radiochim. Acta* **2000**, *88*, 633−637.
[61] *Proceedings of the Workshop on Speciation, Techniques and facilities for Radioactive Materials at Sunchrotron Light Sources*, OECD − NEA, 4−6 October **1998**, Grenoble, France and *Proceedings of the 2nd Euroconference and NEA Workshop on Speciation, Techniques and Facilities for Radioactive Materials at Synchrotron Light Sources* **2001**, Grenoble, France.
[62] H. Konishi, A. Yokoya, H. Shiwaku, H. Motohashi, T. Makita, Y. Kashihara, S. Hashimoto, T. Harami, T. Sasaki, H. Maeta, H. Ohno, H. Maezawa, S. Asaoka, N. Kanaya, K. Ito, N. Usami, K. Kobayashi, *Nucl. Instrum. Methods Phys. Res.* **1996**, *372*, 322−332.
[63] T. Nakatani, Y. Saitoh, Y. Teraoka, T. Okane, A. Yokoya, *J. Synchrotron Radiat.* **1998**, *5*, 536−538.
[64] M. O. Kraus, J. H. Oliver, *J. Phys. Chem. Ref. Data* **1979**, *8*, 329−338.
[65] R. Revel, C. Den Auwer, C. Madic, F. David, B. Fourest, S. Hubert, J. F. Le Du, L. R. Morss, *Inorg. Chem.* **1999**, *38*, 4139−4141.
[66] C. Den Auwer, M. C. Charbonnel, M. G. B. Drew, M. Grigoriev, M. J. Hudson, P. B. Iveson, C. Madic, M. Nierlich, M. T. Presson, R. Revel, M. L. Russel, P. Thuéry, *Inorg. Chem.* **2000**, *39*, 1487−1495.
[67] V. Vallet, U. Wahlgren, B. Schimmelpfennig, H. Moll, Z. Szabo, I. Grenthe, *Inorg. Chem.* **2001**, *40*, 3516−3525.
[68] A. L. Ankudinov, B. Ravel, J. J. Rehr, S. D. Conradson, *Phys. Rev. B* **1998**, *58*, 7565−7576.
[69] A. L. Ankudinov, S. D. Conradson, J. Mustre de Leon, J. J. Rehr, *Phys. Rev. B* **1998**, *57*, 7518−7525.
[70] F. de Groot, *Chem. Rev.* **2001**, *101*, 1779−1808.
[71] J. M. Lawrence, M. L. den Boer, R. D. Parks, J. L. Smith, *Phys. Rev. B* **1984**, *29*, 568−575.
[72] J. Petiau, G. Calas, D. Petitmaire, A. Bianconi, M. Benfatto, A. Marcelli, *Phys. Rev. B* **1986**, *34*, 7350−7361.
[73] G. Kalkowski, G. Kaindl, S. Bertram, G. Schmiester, J. Rebizant, J. C. Spirlet, O. Vogt, *Solid State Commun.* **1987**, *64*, 193−196.
[74] G. Kalkowski, G. Kaindl, W. D. Brewer, W. Krone, *Phys. Rev. B* **1987**, *35*, 2667−2677.
[75] J. Guo, D. E. Ellis, E. L. Soderholm, G. K. Shenoy, *Phys. Rev. B* **1989**, *39*, 6125−6139.
[76] F. Jollet, T. Petit, S. Gota, N. Thromat, M. Gautier-Soyer, A. Pasturel, *J. Phys.: Condens. Matter* **1997**, *9*, 9393−9401.
[77] E. A. Hudson, J. J. Rehr, J. J. Bucher, *Phys. Rev. B* **1995**, *52*, 13815−13826.
[78] E. A. Hudson, P. G. Allen, L. J. Terminello, M. A. Denecke, T. Reich, *Phys. Rev. B* **1996**, *54*, 156−165.
[79] A. L. Ankudinov, A. I. Nesvizhskii, J. J. Rehr, *J. Synchrotron Radiat.* **2001**, *8*, 92−95.
[80] S. E. Shadle, B. Hedman, K. O. Hodgson, E. I. Solomon, *J. Am. Chem. Soc.* **1995**, *117*, 2259−2272.
[81] V. Briois, C. Cartier dit Moulin, P. Sainctavit, C. Brouder, A. M. Flank, *J. Am. Chem. Soc.* **1995**, *117*, 1019−1026.
[82] V. Briois, P. Sainctavit, G. J. Long, F. Grandjean, *Inorg. Chem.* **2001**, *40*, 912−918.

[83] C. Den Auwer, E. Simoni, S. D. Conradson, J. Mustre de Leon, P. Moisy, A. Bérès, *C. R. Acad. Sci., Ser. IIc: Chim.* **2000**, *3*, 327−333.
[84] C. Den Auwer, E. Simoni, R. Drot, M. Gailhanou, S. D. Conradson, J. Mustre de Leon, *New J. Chem.* **2003**, *27*, 648−655.
[85] C. Den Auwer, C. Lecouteux, M. C. Charbonnel, C. Madic, R. Guillaumont, *Polyhedron* **1997**, *16*, 2233−2238; C. Den Auwer, M. C. Charbonnel, M. T. Presson, C. Madic, R. Guillaumont, *Polyhedron* **1998**, *17*, 4507−4517.
[86] D. Meyer, S. Fouchard, E. Simoni, C. Den Auwer, *Radiochim. Acta* **2002**, *90*, 253−258.
[87] D. H. Templeton, L. K. Templeton, *Acta Crystallogr., Sect. A* **1982**, *38*, 62−67.
[88] S. D. Conradson, I. Al Mahamid, D. L. Clark, N. J. Hess, E. A. Hudson, M. P. Neu, P. D. Palmer, W. H. Runde, C. Drew Tait, *Polyhedron* **1998**, *17*, 599−601.
[89] E. Simoni, H. Abazli, A. Cousson, M. Pagès, *Radiochem. Radioanal. Lett.* **1981**, *49*, 37−40.
[90] J. Rakovan, R. J. Reeder, E. J. Elzinga, D. J. Cherniak, C. Drew Tait, D. E. Morris, *Environ. Sci. Technol.* **2002**, *36*, 3114−3117.
[91] J. Mustre de Leon, S. D. Conradson, D. L. Clark, C. Den Auwer, N. Hess, D. W. Keogh, P. D. Palmer, E. Simoni, D. Blanchard, to be submitted.
[92] E. Simoni, M. Louis, S. Hubert, S. Xia, *Opt. Mater.* **1995**, *4*, 641 −650.
[93] A. J. Francis, C. J. Dodge, F. Lu, G. P. Halada, C. R. Clayton, *Environ. Sci. Technol.* **1994**, *28*, 636−639.
[94] C. W. Williams, J-P. Blaudeau, J. C. Sullivan, M. R. Antonio, B. Bursten, L. Soderholm, *J. Am. Chem. Soc.* **2001**, *123*, 4346−4347.
[95] P. Jolivet, C. Den Auwer, E. Simoni, *J. Nucl. Mater.* **2002**, *301*, 142−152.
[96] M. A. Denecke, *Proceedings of the Workshop on Speciation, Techniques and Facilities for Radioactive Materials at Sunchrotron Light Sources*, OECD − NEA, 4−6 October **1998**, Grenoble, France.
[97] S. Spencer, L. Gagliardi, N. C. Handy, A. G. Ioannou, C-K. Skylaris, A. Willetts, A. M. Simper, *J. Phys. Chem. A* **1999**, *103*, 1831−1837.
[98] L. Gagliardi, B. O. Roos, *Inorg. Chem.* **2002**, *41*, 1315−1319.
[99] L. Sémon, C. Boehme, I. Billard, C. Hennig, K. Lützenkirchen, T. Reich, A. Roβberg, I. Rossini, G. Wipff, *ChemPhysChem* **2001**, *2*, 591−598.
[100] U. Wahlgren, H. Moll, I. Grenthe, B. Schimmelpfennig, L. Maron, V. Vallet, O. Gropen, *J. Phys. Chem. A* **1999**, *103*, 8257−8264.
[101] C. Den Auwer, R. Revel, M. C. Charbonnel, M. T. Presson, S. D. Conradson, E. Simoni, J. F. Le Du, C. Madic, *J. Synchrotron Rad.* **1999**, *6*, 101−104.
[102] D. L. Clark, S. D. Conradson, R. J. Donohoe, D. W. Keogh, D. E. Morris, P. D. Palmer, R. D. Rogers, C. Drew Tait, *Inorg. Chem.* **1999**, *38*, 1456−1466.
[103] P. Charpin, A. Dejean, G. Folcher, P. Rigny, P. Navaza, *J. Chim. Phys. (Paris)* **1985**, *82*, 925−932.
[104] H. A. Thompson, G. E. Brown, Jr., G. A. Parks, *Am. Mineral.* **1997**, *82*, 483−496.
[105] P. G. Allen, J. J. Bucher, D. K. Shuh, N. M. Edelstein, T. Reich, *Inorg. Chem.* **1997**, *36*, 4676−4683.
[106] A. J. Dent, J. D. Ramsay, S. W. Swanton, *J. Colloid Interface Sci.* **1992**, *150*, 45−60.
[107] C. Chisholm-Brause, S. D. Conradson, C. T. Buscher, P. G. Eller, D. E. Morris, *Geochim. Cosmoschim. Acta* **1994**, *58*, 3625−3631.
[108] H. Moll, T. Reich, Z. Szabo, *Radiochim. Acta* **2000**, *88*, 411−415.
[109] J-M Combes, C. J. Chisholm-Brause, G. E. Brown, Jr., G. A. Parks, S. Conradson, P. G. Eller, I. R. Triay, D. E. Hobart, A. Meijer, *Environ. Sci. Technol.* **1992**, *26*, 376−382.
[110] M. R. Antonio, L. Soderholm, C. W. Williams, J-P. Blaudeau, B. E. Bursten, *Radiochim. Acta* **2001**, *89*, 17−25.
[111] P. J. Panak, C. H. Booth, D. L. Caulder, J. J. Bucher, D. K. Shuh, H. Nitsche, *Radiochim. Acta* **2002**, *90*, 315−321.
[112] N. N. Krot, A. D. Gelman, *Dokl. Akad. Nauk SSSR* **1967**, *177*, 124.
[113] M. S. Grigoriev, B. F. Gulev, N. N. Krot, *Radiochemistry* **1986**, *28*, 630−634.
[114] V. P. Shilov, *Radiochemistry* **1998**, *40*, 11−16.
[115] D. L. Clark, S. D. Conradson, M. P. Neu, P. D. Palmer, W. Runde, C. Drew Tait, *J. Am. Chem. Soc.* **1997**, *119*, 5259−5260.
[116] H. Bolvin, U. Wahlgren, H. Moll, T. Reich, G. Geipel, T. Fanghänel, I. Grenthe, *J. Phys. Chem. A* **2001**, *105*, 11441−11445.
[117] L. Soderholm, M. R. Antonio, C. W. Williams, J. C. Sullivan, S. R. Wasserman, J-P. Blaudeau, *Second Euroconference and NEA Workshop on Speciation, Techniques and Facilities for Radioactive Materials at Synchrotron Light Source*, September 10−12, **2000**, Grenoble, France.
[118] S. D. Conradson, R. J. Donohoe, D. W. Keogh, D. E. Morris, P. D. Palmer, B. L. Scott, C. Drew Tait, manuscript in preparation; D. L. Clark, S. D. Conradson, R. J. Donohoe, D. W. Keogh, D. E. Morris, P. D. Palmer, B. L. Scott, C. Drew Tait, manuscript in preparation.
[119] W. Runde, M. P. Neu, S. D. Conradson, D. L. Clark, P. D. Palmer, S. D. Reilly, B. L. Scott, C. D. Tait, *Mat. Res. Soc. Symp. Proc.* **1997**, *465*, 693−703.
[120] P. G. Allen, J. J. Bucher, D. L. Clark, N. M. Edelstein, S. A. Ekberg, J. W. Gohdes, E. A. Hudson, N. Kaltsoyannis, W. W. Lukens, M. P. Neu, P. D. Palmer, T. Reich, D. K. Shuh, C. D. Tait, B. D. Zwick, *Inorg. Chem.* **1995**, *34*, 4797−4807.
[121] T. I. Docrat, J. F. W. Mosselmans, J. M. Charnock, M. W. Whiteley, D. Collison, F. R. Livens, C. Jones, M. J. Edmiston, *Inorg. Chem.* **1999**, *38*, 1879−1882.
[122] G. Bernhard, G. Geipel, T. Reich, V. Brendler, S. Amayri, H. Nitsche, *Radiochim. Acta* **2001**, *89*, 511−518.
[123] D. L. Clark, S. D. Conradson, S. A. Ekberg, N. J. Hess, D. R. Janecky, M. P. Neu, P. D. Palmer, C. Drew Tait, *New J. Chem.* **1996**, *20*, 211−220.
[124] D. L. Clark, S. D. Conradson, S. A. Ekberg, N. J. Hess, M. P. Neu, P. D. Palmer, W. Runde, C. Drew Tait, *J. Am. Chem. Soc.* **1996**, *118*, 2089−2090.
[125] D. L. Clark, D. E. Hobart, M. P. Neu, *Chem. Rev.* **1995**, *95*, 25−48.
[126] H. Moll, T. Reich, C. Henning, A. Roβberg, Z. Szabo, I. Grenthe, *Radiochim. Acta* **2000**, *88*, 559−566.
[127] M. A. Denecke, S. Pompe, T. Reich, H. Moll, M. Bubner, K. H. Heise, R. Nicolai, H. Nitsche, *Radiochim. Acta* **1997**, *79*, 151−159.
[128] S. Pompe, M. Bubner, M. A. Denecke, T. Reich, A. Brachmann, G. Geipel, R. Nicolai, K. H. Heise, H. Nitsche, *Radiochim. Acta* **1996**, *74*, 135−140.
[129] M. A. Denecke, T. Reich, S. Pompe, M. Bubner, K. H. Heise, H. Nitsche, P. G. Allen, J. J. Bucher, N. M. Edelstein, D. K. Shuh, K. R. Czerwinski, *Radiochim. Acta* **1998**, *82*, 103−108.
[130] A. Roβberg, L. Baraniak, T. Reich, C. Hennig, G. Bernhard, H. Nitsche, *Radiochim. Acta* **2000**, *88*, 593−597.
[131] C. Hennig, P. J. Panak, T. Reich, A. Roβberg, J. Raff, S. Selenska-Pobell, W. Matz, J. J. Bucher, G. Bernhard, H. Nitsche, *Radiochim. Acta* **2001**, *89*, 625−631.
[132] J. H. Burns, G. M. Brown, R. R. Ryan, *Acta Crystallogr., Sect. C* **1985**, *41*, 1446−1448.
[133] P. Charpin, M. Lance, M. Nierlich, D. Vigner, *Acta Crystallogr., Sect. C* **1986**, *42*, 560−563.
[134] P. Charpin, M. Lance, M. Nierlich, D. Vigner, *Acta Crystallogr., Sect. C* **1987**, *43*, 231−233.
[135] C. Den Auwer, M. C. Charbonnel, M. T. Presson, unpublished data.
[136] N. Condamines, C. Musikas, *Solvent Extr. Ion Exch.* **1992**, *10*, 69−100.
[137] J. R. Bargar, R. Reitmeyer, J. J. Lenhart, J. A. Davis, *Geochim. Cosmoschim. Acta* **2000**, *64*, 2737−2749.
[138] P. Dähn, A. M. Scheidegger, A. Manceau, E. Curti, B. Baeyens,

M. H. Bradbury, D. Chateigner, *J. Colloid Interface Sci.* **2002**, *249*, 8−21.
[139] L. N. Moyes, M. J. Jones, W. A. Reed, F. R. Livens, J. M. Charnock, J. F. W. Mosselmans, C. Hennig, D. J. Vaughan, R. A. D. Pattrick, *Environ. Sci. Technol.* **2002**, *36*, 179−183.
[140] M. A. Denecke, J. Rothe, K. Dardenne, P. Lindqvist-Reis, *Phys. Chem. Chem. Phys.* **2003**, *5*, 939−946.
[141] J. R. Bargar, R. Reitmeyer, J. A. Davis, *Environ. Sci. Technol.* **1999**, *33*, 2481−2484.
[142] R. Drot, E. Simoni, C. Den Auwer, *C. R. Acad. Sci., Ser. IIc: Chim.* **1999**, *2*, 111−117.
[143] G. N. Greaves, N. T. Barrett, G. M. Antonini, F. R. Thornley, B. T. M. Willis, A. Steel, *J. Am. Chem. Soc.* **1989**, *111*, 4313−4324.
[144] L. N. Moyes, R. H. Parkman, J. M. Charnock, D. J. Vaughan, F. R. Livens, C. R. Hugues, A. Braithwaite, *Environ. Sci. Technol.* **2000**, *34*, 1062−1068.
[145] R. J. Reeder, M. Nugent, G. M. Lamble, C. D. Tait, D. E. Morris, *Environ. Sci. Technol.* **2000**, *34*, 638−644.
[146] A. M. Scheidegger, G. M. Lamble, D. L. Sparks, *J. Colloid Interface Sci.* **1997**, *186*, 118−128.
[147] S. N. Towle, G. E. Brown, Jr., G. A. Parks, *J. Colloid Interface Sci.* **1999**, *217*, 299−311.
[148] S. N. Towle, J. R. Bargar, G. E. Brown, Jr., G. A. Parks, *J. Colloid Interface Sci.* **1999**, *217*, 312−321.
[149] T. P. Trainor, J. P. Fitts, A. S. Templeton, D. Grolimund, G. E. Brown, Jr., *J. Colloid Interface Sci.* **2001**, *244*, 239−244.
[150] T. D. Waite, J. A. Davis, T. E. Payne, G. A. Waychunas, N. Xu, *Geochim. Cosmochim. Acta* **1994**, *58*, 5465−5478.
[151] T. Reich, H. Moll, T. Arnold, M. A. Denecke, C. Hennig, G. Geipel, G. Bernhard, H. Nitsche, P. G. Allen, J. J. Bucher, N. M. Edelstein, D. K. Shuh, *J. Electron Spectrosc. Relat. Phenom.* **1998**, *96*, 237−243.
[152] A. Manceau, L. Charlet, M. C. Boisset, B. Didier, L. Spadini, *Appl. Clay Sci.* **1992**, *7*, 201−223.
[153] C. Hennig, T. Reich, R. Dähn, A. M. Scheidegger, *Radiochim. Acta* **2002**, *90*, 653−657.
[154] C. Lomenech, E. Simoni, R. Drot, J.-J. Ehrardt, J. Mielczarski, *J. Colloid Interface Sci.* **2003**, *261/262*, 221−232.
[155] E. R. Sylwester, E. A. Hudson, P. G. Allen, *Geochim. Cosmochim. Acta* **2000**, *64*, 2431−2438.
[156] E. Ordoñez-Regil, R. Drot, E. Simoni, J-J. Ehrhardt, *Langmuir* **2002**, *18*, 7977−7984.
[157] J. R. Bargar, G. E. Brown Jr., G. A. Parks, *Geochim. Cosmochim. Acta* **1998**, *62*, 193−207.
[158] P. H. Citrin, *Phys. Rev. B* **1985**, *31*, 700−721.
[159] G. E. Brown, Jr., V. E. Henrich, W. H. Casey, D. L. Clark, C. Eggleston, A. Felmy, D. W. Goodman, M. Grätzel, G. Maciel, M. I. McCarthy, K. H. Nealson, D. A. Sverjensky, M. F. Toney, J. M. Zachara, *Chem. Rev.* **1999**, *99*, 77−174.

Received February 17, 2003

